Summer 5-31-2022

Petrographic and Geochemical Records of Climate Perturbation in Carbonates from a Perennially Ice-Covered Antarctic Lake

Jared Clance
University of New Mexico

Jared Clance
Candidate

Earth & Planetary Sciences
Department

This thesis is approved, and it is acceptable in quality and form for publication:

Approved by the Thesis Committee:

Tyler Mackey , Chairperson

Laura Crossey

Corinne Myers

Cristina Takacs-Vesbach

PETROGRAPHIC AND GEOCHEMICAL RECORDS OF CLIMATE PERTURBATION IN CARBONATES FROM A PERENNIALLY ICE-COVERED ANTARCTIC LAKE

BY

JARED CLANCE

B.S. (University of Tennessee, Knoxville) 2020

THESIS

Submitted in Partial Fulfillment of the Requirements for the Degree of

Master of Science

in

Earth and Planetary Sciences

The University of New Mexico

Albuquerque, New Mexico

July 2022

Acknowledgements

I would like to thank my advisor, Tyler Mackey, for his exceptional mentorship throughout the course of my thesis work. His guidance over the past two years has made this work possible and greatly bolstered my confidence as I learned and navigated through a field of study in which I had very little prior experience. I would also like to thank the other members of my committee: Cori Myers, Laura Crossey, and Cristina Takacs-Vesbach, who have all helped me develop my academic and professional career in various ways.

This work would not have been successful without the assistance of many others at UNM. The collection and interpretation of the data I present here were made possible by the members of the analytical geochemistry laboratory, the Institute of Meteoritics, and the Center for Stable Isotopes at UNM; in particular, I would like to thank Mike Spilde, Mehdi Ali, Zach Sharp, Viorel Atudorei, and Nathan Perdue for their contributions to my research.

Finally, I am very thankful for all the support I have received from the rest of the Mackey lab group and the Earth & Planetary Sciences department as a whole, as well as that of my friends and family who have provided countless forms of encouragement and support throughout my time in this program.

Funding for this thesis came from the UNM Department of Earth & Planetary Sciences Albert and Mary Jane Black and E.E.E. Graduate Assistantship, start-up funding for the Mackey lab, the UNM WeR1 faculty summer support program, and the NSF Division of Polar Programs award number 1115245.

PETROGRAPHIC AND GEOCHEMICAL RECORDS OF CLIMATE PERTURBATION IN CARBONATES FROM A PERENNIALLY ICE-COVERED ANTARCTIC LAKE

by

Jared Clance

B.S., Biological Sciences, University of Tennessee, Knoxville, 2020

M.S., Earth and Planetary Sciences, University of New Mexico, 2022

ABSTRACT

Carbonate precipitation in perennially ice-covered Lake Fryxell, McMurdo Dry Valleys, Antarctica produces a modern analog for Antarctic paleolake carbonates. Lake Fryxell contains a steep oxycline in the photic zone, where dissolved oxygen falls from supersaturation to zero. In the lake's benthic microbial mats, oxygen concentrations are higher than in the water column due to microbial photosynthesis. These mats contain carbonate cements that precipitated in a discrete episode from mat pore waters. Precipitation continued through seasonal fluctuations in oxygenation, demonstrated by variable concentrations of oxidized and reduced manganese and iron within carbonates. Carbonates precipitated out of isotopic equilibrium with the lake water column and are enriched in ^{18}O relative to expected values. Carbonate $\delta^{18}O$ varies by >20‰ across μm to mm; carbonate triple oxygen isotopes suggest mixing of a modified marine water with lake water as an explanation for both isotopic heterogeneity and a possible trigger for this episodic carbonate precipitation.

Table of Contents

Acknowledgements ..... **iii**

Abstract ..... **iv**

Table of Contents ..... **v**

List of Tables ..... **vii**

List of Figures ..... **viii**

Introduction **1**

Background **3**

History of Taylor Valley 3
Lake Fryxell 4
Lake Fryxell Water Chemistry 5
Lake Fryxell Biology 7
Biogeochemical Proxies in Lake Fryxell Carbonates 8

Methods and Materials **10**

Sample Collection 10
Sample Selection and Preparation 10
X-Ray Diffraction 11
Petrography 12
Cathodoluminescence 12
Stable Isotope Analysis 13
Elemental Composition Analysis 16

Results **18**

Spatial Distribution of Carbonates 18
X-Ray Diffraction 18
Petrography 18
Cathodoluminescence 19
Elemental Composition 21
Manganese Oxides 22
Stable Isotopes 22

Summary and Discussion **24**

Summary 24
Distribution of Lake Fryxell Carbonates 24
Carbonate Precipitation Timing in Lake Fryxell 26
Redox Geochemistry of Lake Fryxell Carbonates 27
Isotope Geochemistry of Lake Fryxell Carbonates 31

Conclusions 37

Tables 40

Figures 42

Appendices 59

Appendix A: Supplementary Data & Figures 60

References 68

List of Tables

Table 1. Measurements of depth to carbonate from the microbial mat-water interface.

Table 2. List and descriptions of samples used in this study.

Table 3. Accepted $\delta^{13}C$ and $\delta^{18}O$ values of isotopic standards used in this study.

Table 4. Composition and Fe/Mn concentrations of ICP-OES standards used in this study.

Table 5. $\delta^{18}O$, $\delta^{17}O$, and $\Delta^{17}O$ values of Lake Fryxell carbonates.

Table S1. $\delta^{13}C$ and $\delta^{18}O$ values of Lake Fryxell carbonates from traditional stable isotope analysis.

Table S2. Mn and Fe concentration data from LA-ICP-OES.

List of Figures

Figure 1. Map of Antarctica showing the McMurdo Dry Valleys, Ross Ice Shelf, Taylor Valley, and Lake Fryxell.

Figure 2. Geochemical profile of the Lake Fryxell water column and dissolved oxygen profile across the microbial mat-water interface.

Figure 3. Profile of manganese and iron concentrations in the Lake Fryxell water column.

Figure 4. X-ray diffraction spectra for carbonate samples from the top and bottom ends of the depth transect.

Figure 5. Transmitted-light photomicrographs of thin sections showing the most common crystal morphologies in Lake Fryxell carbonates.

Figure 6. Transmitted-light photomicrographs showing botryoidal arrangements of acicular calcite crystals.

Figure 7. Cathodoluminescence images showing characteristic luminescence patterns at five depths in the oxycline.

Figure 8. Cathodoluminescence images showing concentric arrangements of alternating bright and dark zones, and transmitted-light photomicrographs of the same areas.

Figure 9. Cathodoluminescence images of dimly- to non-luminescent zones at the oxic-anoxic transition depth, and transmitted-light photomicrographs of the same areas.

Figure 10. Log-log plot of Mn and Fe concentrations of Lake Fryxell carbonates, determined by LA-ICP-OES, with corresponding cathodoluminescence brightness at each sampling site.

Figure 11. Mn concentrations of carbonates by depth with corresponding cathodoluminescence brightness at each sampling site.

Figure 12. Fe concentrations of carbonates by depth with corresponding cathodoluminescence brightness at each sampling site.

Figure 13. Cathodoluminescence bands in carbonate from 9.3 m depth and Fe/Mn concentrations in a transect across the zone in the direction of crystal growth.

Figure 14. Scanning electron micrograph of manganese oxide spheroids entombed in calcite at the oxic-anoxic transition depth.

Figure 15. Averaged $\delta^{13}C$ values of carbonate samples compared to values calculated for precipitation in isotopic equilibrium with the DIC pool.

Figure 16. Measured $\delta^{13}C$ and $\delta^{18}O$ values with cathodoluminescence brightness at each sampling site.

Figure 17. $\delta^{17}O_{calcite}$ vs. $\delta^{18}O_{calcite}$ of Lake Fryxell carbonates compared to expected values based on the accepted mass-dependent fractionation ratio $\delta^{17}O/\delta^{18}O = 0.528$.

Figure 18. $\Delta'^{17}O_{calcite}$ vs. $\delta'^{18}O_{calcite}$ of Lake Fryxell carbonates.

Figure 19. Lake Fryxell calcite $\delta^{18}O$ compared to predicted $\delta^{18}O$ of calcite precipitating in equilibrium with various water sources in the McMurdo Dry Valleys.

Figure S1. Paragenetic sequence diagram summarizing seasonal redox changes in Lake Fryxell pore waters.

Figure S2. SEM-EDS maps showing abundances of various elements at the surface of a piece of calcite, including an Mn- and Fe-bearing oxide entombed in carbonate.

Figure S3. Schematic diagram of subsurface brine-saturated sediments in Taylor Valley which connect Lake Fryxell to the ocean.

Figure S4. Reflected-light photomicrographs of carbonate billets showing $\delta^{18}O$ values at individual subsampling sites.

Figure S5. Electron microprobe transect across CL bands in carbonate from 9.3 m, showing variability in Fe and Mn concentrations and Fe/Mn ratio.

I. Introduction

Paleolake carbonate deposits are rich natural archives of climate change, preserving "snapshots" of environmental conditions within lake waters and their surroundings. Lacustrine carbonates can contain a wealth of information concerning changing climate and biogeochemistry via a wide variety of physical and geochemical proxies, often enabling detailed reconstruction of past environmental conditions and short- to long-term changes therein (e.g. Clayton-Greene et al. 1988, Hawes et al. 2011, Mackey et al. 2018). However, processes like diagenesis and weathering can alter these deposits through time, corrupting or erasing these proxies. Thus, it is helpful to examine modern lacustrine carbonates as analogs for their ancient counterparts in order to resolve these issues of preservation. In the McMurdo Dry Valleys of Antarctica (MDV), modern and ancient lacustrine carbonate deposits provide a long-term record of dramatic changes in local climate, including significant glaciation/deglaciation and lake level changes on the order of hundreds of meters during the Last Glacial Maximum (LGM) and subsequent warming (Hall et al. 2015, Myers et al. 2021).

One understudied suite of modern Antarctic lacustrine carbonates is contained in the benthos of perennially ice-covered Lake Fryxell in Taylor Valley, MDV. Lake Fryxell is meromictic, with a stable density-stratified water column and metabolically active benthic microbial mats. Calcium carbonates precipitate from the waters of Lake Fryxell in close spatial association with these microbial mats, providing a modern analog for microbe-mineral systems as likely existed in polar and other cold-climate paleolakes, such as Glacial Lake Washburn, which occupied Taylor Valley during the late Pleistocene to early Holocene (Hall et al. 2000, Myers et al. 2021). Because these carbonates form in association with metabolically active microbes, investigation of their utility as paleoclimate records must take

the effects of metabolic processes into account alongside the geochemistry of the lake itself. In this study, the petrography and geochemistry of Lake Fryxell carbonates are investigated in order to describe the roles of biology and climate perturbations in carbonate precipitation and geochemistry, and the utility of these carbonates as a record of climate change in the MDV.

II. Background

i. History of Taylor Valley

Taylor Valley is one of several ice-free valleys in the MDV, lying between the Asgard Range and Kukri Hills mountains and terminating at the McMurdo Sound. The valley has been the site of extensive ice sheet advance and retreat during the past 20,000 years (Lawrence and Hendy 1989, Myers et al. 2021). Ice from the Ross Ice Sheet advanced into the MDV during the LGM (28.5-12.8 years BP) when local mean annual air temperatures were 4-9 ℃ lower than modern (Steig et al. 2000). This ice formed a glacial dam in Taylor Valley which reached a maximum elevation of 300-350 meters above sea level (m.a.s.l.) around 13,000 years BP and allowed the formation of a large paleolake, Glacial Lake Washburn (GLW), which filled all of Taylor Valley (Lawrence and Hendy 1989, Hall and Denton 2000, Myers et al. 2021). Lake levels in Taylor Valley have undergone drastic changes of hundreds of meters since the LGM; retreat of the ice dam due to warming after the LGM caused drainage of GLW and lowered lake levels to 78-81 m.a.s.l., as water became limited by a sill near the edge of the McMurdo Sound (Myers et al. 2021). Lake levels fell further after the retreat of the Ross ice sheet, likely due to rates of evaporation exceeding melt water influx. Lake basins have subsequently refilled with glacial melt waters, and lake levels throughout Taylor Valley have been rising since the initial observations of the valley in 1903 during Scott's first Antarctic expedition (Scott 1905, Lawrence and Hendy 1985, Harnish et al. 1991, Jungblut et al. 2016).

ii. Lake Fryxell

Lake Fryxell is a perennially ice-covered meromictic lake located in Taylor Valley. Of the lakes in Taylor Valley, Lake Fryxell is located the closest to the ocean, approximately 5 km from the McMurdo Sound (Figure 1) (Mikucki et al. 2015). The lake has a surface area of 7.5 km^2, and its depth increases gradually along a gently-sloping floor (Sumner et al. 2015, Jungblut et al. 2016). Lake Fryxell is a closed basin lake with its level determined by the balance between melt water influx and loss by evaporation or sublimation of the ice cover (Lawrence and Hendy 1985, Dugan et al. 2013). About 1000 years BP, following the contraction of GLW, high evaporation rates created a shallow sodium chloride brine in the Fryxell basin (Lawrence and Hendy 1989). Lake Fryxell was then refilled with glacial melt waters to its present depth (Lawrence and Hendy 1989). The lake level has risen gradually in recent decades, from 17 m in the year 2001 to its present depth of 18.3 m (Doran and Gooseff 2020).

Lake Fryxell has a 4-5 meter-thick ice cover which persists year-round (Priscu 2018). This ice cover strongly influences physical and chemical features of the lake by preventing wind-driven mixing and gas exchange with the atmosphere, resulting in a stable density-stratified water column in which solute movement is primarily limited by diffusion and conductivity increases steadily with depth (Jungblut et al. 2016, Lawrence and Hendy 1985).

The lake experiences approximately four months of constant darkness during the austral winter and four months of constant sunlight during the summer. Sunlight is strongly attenuated by the ice cover, with less than 3% of incident photosynthetically active radiation (PAR) reaching the water column (Priscu 2021), where it facilitates oxygenic photosynthesis by cyanobacteria in the microbial mats present on much of the lake floor (see subsection iv)

(Jungblut et al. 2016, Dillon et al. 2020). The upper portion of the water column is supersaturated with dissolved oxygen (DO) due to a combination of input from 13 glacial melt streams which flow during the summer, microbial oxygenic photosynthesis, and exclusion of dissolved gases from the ice cover (Craig et al. 1992). A steep oxycline exists between 8-10 meters depth; below 9.8 meters, the water column is euxinic and oxygen is present only within microbial mats, which remain photosynthetically active as deep as 10.5 meters (Figure 2) (Sumner et al. 2015, Jungblut et al. 2016, Dillon et al. 2020a).

iii. Lake Fryxell Water Chemistry

The water column of Lake Fryxell is stratified by density with respect to most solutes due to prevention of wind-driven mixing by the ice cover. Water immediately below the ice cover is fresh, with conductivity <1 mS/cm, and conductivity increases steadily to approximately 8 mS/cm near the bottom of the lake (Jungblut et al. 2016). Concentrations of most major solutes in Lake Fryxell increase consistently with depth, with the notable exception of [Ca^{2+}], which remains comparatively low (<100 ppm) throughout the water column due to removal via calcium carbonate precipitation (Lawrence and Hendy 1985, Jungblut et al. 2016).

Dissolved oxygen (DO) concentration in Lake Fryxell exhibits large fluctuations throughout the water column. Exclusion of gasses from the ice cover during freezing allows gas buildup to the point of supersaturation in shallow waters; DO rapidly increases from 15-20 mg/L above 6.5 meters depth to a peak of about 33 mg/L at 8.2 meters, below which DO rapidly disappears from the water column, falling below saturation around 9.3 meters and becoming completely absent from the water column by 10 meters (Jungblut et al. 2016, Dillon et al. 2020a). Maximum planktonic chlorophyll concentrations are present around the

oxycline, indicating a peak in primary productivity within this depth range (Roberts et al. 2000, Dillon et al. 2020b). Partial pressure of oxygen (pO_2) fluctuates over the course of the austral summer, reaching a maximum in mid-summer (Lawrence and Hendy 1985). Changes in microbial photosynthetic rates throughout the season likely contribute to this fluctuation; photosynthesis leads to elevated DO concentrations in microbial mats and mat pore waters (Sumner et al. 2015, Figure 1B), and some of this oxygen is released to the water column, as is evidenced by increased DO concentrations in the water millimeters above the mat-water interface (Sumner et al. 2015).

Dissolved inorganic carbon (DIC) is present in concentrations of hundreds of mg/L within the oxycline and is dominated by HCO_3^- due to the pH of 7.4-7.5 in this depth range (Jungblut et al. 2016, Priscu 2019). The $\delta^{13}C_{DIC}$ profile follows a similar pattern to the DO and chlorophyll profiles; $\delta^{13}C_{DIC}$ increases from near zero just below the ice cover to a maximum of 3-4‰ VPDB around 8 meters, then decreases to approximately -4‰ near the lake bottom (Knoepfle et al. 2009). This is interpreted as a result of microbial activity; preferential uptake of ^{12}C during oxygenic photosynthesis in combination with a lack of water column mixing results in the strongest $^{13}C_{DIC}$ enrichment at the same depth at which maximum photosynthetic activity occurs (Neumann et al. 1998, Neumann et al. 2004).

$\delta^{18}O_{water}$ is fairly constant throughout the water column of Lake Fryxell, with a narrow range of -31.94 to -31.29‰ VPDB (Dowling and Lyons 2014). Because of this consistency in $\delta^{18}O_{water}$, departures of $\delta^{18}O_{calcite}$ from values predicted by typical calcite-water fractionation may be useful indications of historical changes in physical and chemical factors such as temperature, pH, precipitation rate, and the source(s) of the water from which the carbonates precipitated (Watkins et al. 2013, Watkins et al. 2014, Mackey et al. 2018).

Changes in $\delta^{18}O$ of these carbonates across depth and/or at different points in time may help describe the geochemical history of Lake Fryxell and changes in local climate through time.

iv. Lake Fryxell Biology

Lake Fryxell hosts abundant benthic microbial mats, which cover most of the lake floor at oxic depths. Photosynthetically active mats extend a short depth into the anoxic portion of the lake (Sumner et al. 2015). The mats exhibit different morphologies at different depths, from well-structured pinnacles and ridges in shallower waters to unconsolidated flocculent biomass below the oxic-anoxic transition (Jungblut et al. 2016). Mat community composition is dominated by a few genera of cyanobacteria including *Phormidium* and *Leptolyngbya*, with lower abundances of anoxygenic phototrophs, heterotrophs, and diatoms; community composition is strongly influenced by the availability of oxygen and PAR (Jungblut et al. 2016, Dillon et al. 2020a). Sulfate-reducing and sulfur-oxidizing bacteria as well as methanogens have been identified in the water column and sediments below 8 meters depth (Karr et al. 2005a, Karr et al. 2005b, Sattley and Madigan 2006).

Mat-associated and planktonic microbes make up the majority of Lake Fryxell's biological assemblage; oligotrophic conditions and the permanent ice cover discourage colonization by large organisms. The lake's planktonic microbial community includes over 20 species of both heterotrophic and autotrophic protozoans, at least four taxa of algae, and several genera of cyanobacteria including *Phormidium* and *Synechococcus* (Laybourn-Parry et al. 1997). The benthic mats host an assemblage of microscopic metazoans including 55 protozoan taxa, two species of rotifers, and one species of tardigrade (Cathey et al. 1981). No macroscopic metazoans are present in Lake Fryxell.

v. Biogeochemical Proxies in Lake Fryxell Carbonates

Calcite precipitates in association with microbial mats in much of the oxic portion of the lake. The depth range where these carbonates occur spans the lake's oxycline and density-stratified gradients of solutes including major ions (Na^+, Mg^{2+}, Cl^-, etc.) nutrients, and transition metals (Lawrence and Hendy 1985, Harnish et al. 1991, Jungblut et al. 2016). As a result, the mat-water-carbonate system in Lake Fryxell provides a "natural laboratory" in which carbonate precipitation in microbial mats can be investigated under a variety of biogeochemical conditions, expanding the lake's utility as a modern analog for paleolake biogeochemistry.

Redox-sensitive transition metals have been identified as potentially useful paleoenvironmental/paleobiological proxies, but their interactions with microbe-associated carbonates remain poorly understood (Zeyen et al. 2019). Lake Fryxell contains manganese and iron in concentrations of tens to hundreds of micrograms per liter, Mn mostly in solution and Fe in particulate, colloidal, and dissolved forms. Both Mn and Fe are present in very low (<50 μg/l) concentrations above the oxycline; the Mn maximum is located within the oxycline while the Fe maximum is located in the anoxic portion of the water column (Figure 3) (Harnish et al. 1991). Reduced (divalent) cations of both Mn and Fe are able to substitute for Ca^{2+} in calcite, while their more oxidized (trivalent and higher) cations cannot (Dromgoole and Walter 1990).

Because the interactions of Mn and Fe with carbonates are redox-dependent, the presence or absence of these metals in calcite functions as an indicator of local redox conditions at the time of deposition. Local redox conditions exert a strong control on the Fe/Mn ratio in carbonates, as the oxidation state of Fe is very oxygen-sensitive while Mn is

unlikely to persist in Lake Fryxell in any state other than Mn^{2+}; Mn is thermodynamically unstable in aqueous solutions at higher oxidation states (3+ and higher), and even in strongly oxidizing environments, Mn oxidation is kinetically slow unless catalyzed by biological processes (Davison 1993). The rapid transition with depth from oxidizing to reducing conditions in Lake Fryxell's oxycline, coupled with the seasonal fluctuations of photosynthesis in the microbial mats, provides an excellent setting in which to investigate the interactions of Mn and Fe with microbial carbonates under different redox conditions across micron- to decimeter-scale distances, as well as the utility of these metals as carbonate record proxies for changes in redox through time.

The stably stratified water column of Lake Fryxell and the depth profiles of oxygenation, redox-sensitive metal concentrations, and stable isotope compositions therein offer a unique depositional environment in which to study records of microbial ecosystems preserved in carbonates. Cathodoluminescence, Mn/Fe content, and stable isotope compositions of Lake Fryxell's microbial mat-associated carbonates help to describe the timing of carbonate precipitation and changes in redox and isotope geochemistry within the lake across both space and time.

III. Methods and Materials

i. Sample Collection

Samples were collected from the benthos of Lake Fryxell in November 2012, following a transect established in 2006. All water depths referenced in this study are based on the water level in 2012. Sampling was performed by divers operating through a hole melted in the ice cover over 8 meters of water near the transect, and samples were collected near marked stations along the transect. Mat biomass and sediments were collected using 3”-diameter acrylic push cores and by removing sections of mat biomass with a spatula and transferring them to plastic boxes *in situ* (see Jungblut et al. 2016, Dillon et al. 2020a, Dillon et al. 2020b). During some dives, depth to carbonate from the mat-water interface was measured by probing mats with a metal wire marked with measurement increments until a hard surface was encountered. Cores and boxes were frozen and stored on ice for the duration of the field season. Samples were shipped frozen to the University of California, Davis and stored frozen; selected samples were later shipped frozen to the University of New Mexico, Albuquerque in 2020 and 2021 and stored below -20 °C.

ii. Sample Selection and Preparation

Samples were selected from the collection of frozen samples described above, as well as dried dissected carbonates from a dredge sample also collected in 2012 (Table 2). These samples represent a range of depths from 9.0 m to 9.7 m, capturing the transition of the water column from oxygen supersaturation to undersaturation as well as the oxic-anoxic transition zone (Sumner et al. 2015, Jungblut et al. 2016, Dillon et al. 2020a). Sample selection was based on spatial relationships of carbonates and microbial mats, appearance of the

carbonates, as well as relevant geochemical parameters (e.g., dissolved oxygen, Mn and Fe concentrations) at each depth point.

Carbonates contained in sediment cores were located by halving the frozen cores. The acrylic core tubes were cut lengthwise using a hand-held rotary cutting tool with a circular diamond-edged blade, then the sediment core was halved along the same line using a water-cooled Hi-Tech Diamond 6" trim saw to expose the interior of the core. After photographing the exposed surfaces and identifying carbonates of interest, carbonate pieces and the surrounding sediments were excised from the cores with the trim saw, then freeze-dried in order to enable removal of the carbonate from the sediment. Halved cores were vacuum-sealed and stored below -20 °C. Dried carbonates were shipped to Spectrum Petrographics in Vancouver, Washington for preparation as thin sections; carbonate pieces which appeared particularly fragile were first embedded in Epo-Tek 301-2 clear epoxy according to manufacturer instructions to prevent damage during shipping. Samples were prepared as thin sections 30 or 80 μm thick and polished to be suitable for cathodoluminescence imaging.

iii. X-Ray Diffraction

X-ray diffraction (XRD) was used to verify the mineralogy of Lake Fryxell carbonates. Four pieces of dried dissected carbonate collected from Lake Fryxell mats were selected, two each from the upper and lower limits of the depth range examined in this study (9.0 m and 9.7 m, respectively). Carbonate samples were selected based on depth and viability for use in other analyses. Carbonates were crushed into powders by hand using a ceramic mortar and pestle, and 230-340 μg of each powder was weighed out for analysis. XRD analysis was performed using a Rigaku SmartLab diffractometer with Cu Kα radiation (wavelength = 1.54059 Å) and a DeteX Ultra detector. Spectra were collected in the 3-150°

2θ range with a step size of 0.02° and a count time of 6°/minute, and the data were analyzed using MDI Jade software.

iv. Petrography

Transmitted- and reflected-light microscopy were performed on thin sections and billets using a Nikon SMZ25 stereo microscope. Examining these samples in both transmitted and reflected light allowed thorough characterization of features of carbonate crystals such as crystal habit, growth direction, changes in coloration, and association with sediments and organic matter. These observations enabled identification of patterns in various aspects of carbonate deposition (e.g. location of precipitation) across the oxycline. This imaging process also served to identify points of interest for other analyses, such as changes in carbonate coloration indicating potential changes in geochemistry which could be investigated using cathodoluminescence microscopy. Extinction patterns of carbonates in thin sections were observed under cross-polarized light using a Nikon Optiphot-POL petrographic microscope.

v. Cathodoluminescence

Cathodoluminescence (CL) microscopy is a powerful tool for investigation of carbonate geochemistry. While not a quantitative compositional analysis, CL imaging is effective in identifying zones of geochemical heterogeneity in carbonate textures. Different elements and their ions may activate or quench CL in different minerals. In calcium carbonates, the most common CL activator is Mn^{2+} and the most common quencher is Fe^{2+}; both of these cations can occupy Ca^{2+} sites in carbonates (Dromgoole and Walter 1990, Braithwaite 2016). In calcite, Mn^{2+} content as low as ~17 ppm causes yellow luminescence,

which becomes orange to red when Fe^{2+} substitution co-occurs. At high Fe/Mn ratios, CL becomes dark red and is eventually extinguished; there is currently no accepted definitive value for the Fe/Mn ratio at which CL is completely extinguished (Hiatt and Pufahl 2014). Since both Mn and Fe are redox-sensitive and will only substitute for Ca^{2+} when reduced (divalent), their presence or absence in calcium carbonates acts as an indicator of redox conditions in the pore water at the time of deposition.

A Luminoscope ELM-2A cold-cathode microscope with a 5x objective lens was used to collect transmitted-light, reflected-light, and CL images of thin sections and billets. All samples were polished to 3 µm before being placed in the Luminoscope chamber under vacuum (P = 30-50 mtorr) and CL images were captured using a voltage of 5.5-6.0 kV to obtain a beam current of 0.7-0.8 mA, with exposure times of 45-90 seconds. The images collected with the Luminoscope were used to identify CL features representing changes in the substitution of Fe and Mn into the carbonates in order to assess spatial and temporal changes in local redox during carbonate precipitation.

vi. Stable Isotope Analysis

Samples for $\delta^{13}C$ and $\delta^{18}O$ analysis were extracted from billets using a hand-held Proxxon Micromot 60/E drill with Kodiak Cutting Tools carbide end mill bits (bit diameters 1/64” and 1/32”). Drilling sites on each billet were selected in order to acquire a suite of samples encompassing carbonates precipitated at different times and under different redox conditions, as indicated by petrographic and CL imaging, respectively. The powdered samples collected by drilling were washed in 0.8-1.0 mL of 30% hydrogen peroxide overnight to remove organic matter, then the peroxide was removed via micropipette and the remaining carbonate powders were dried at 50-70 °C for several hours. Once completely dry,

60 μg to 2 mg of each powder was loaded into Labco Exetainer vials, which were subsequently flushed with helium gas to remove atmospheric CO_2. Four vials each of at least two carbonate standards were included in each analysis; standards for each round of analysis were selected from NBS-19, IAEA CO-8, IAEA CO-9, and an internal Carrara marble standard (equivalent to IAEA 603). Standards were chosen to provide a range of $\delta^{13}C$ and $\delta^{18}O$ values similar to the range of values expected from the Lake Fryxell samples (Table 3). After flushing with helium, approximately 0.1 mL of phosphoric acid was added to each vial through the septum and allowed to react with samples overnight at 25 °C. $\delta^{13}C$ and $\delta^{18}O$ of the resulting CO_2 were measured using a Thermo Scientific Delta V Plus mass spectrometer. Each sample was measured 12 times per analysis run. High-mass (>300 μg) samples were run multiple times to ensure accurate measurements and prevent contamination of subsequent samples.

For triple oxygen isotope analysis, carbonate samples were prepared via drilling, washing with hydrogen peroxide, and drying following the procedure described above. Once dry, 0.6-1.2 mg of each powder was weighed out and placed into glass vials with glass partitions at the bottom separating the lower section of the tube into two compartments. 1 mL of 100% phosphoric acid was added to the tube on the opposite side of the partition from the sample, and the vials were attached to a vacuum line and allowed to degas until a pressure of ≤30 mtorr was achieved; the tubes were occasionally heated with a heat gun for several seconds at a time to encourage degassing of water vapor from the phosphoric acid. After degassing, the valves on the vials were closed and the tubes were removed from the vacuum line. Vials were gently tilted to allow the phosphoric acid to flow over the glass partition and contact the carbonate powder, then placed in a water bath at 25 °C and allowed to react

overnight. The resulting CO_2 was analyzed for $^{18}O/^{16}O$ and $^{17}O/^{16}O$ using an Aerodyne Research TILDAS-CS laser trace gas and isotope analyzer. IAEA 603 and NBS 18 were used as standards. Each sample was measured 12 times per run.

Bulk samples were also prepared for triple oxygen analysis. Carbonate pieces were selected from freeze-dried samples from multiple depths and ground into powder by hand using a ceramic mortar and pestle. Powders were washed in 30% hydrogen peroxide overnight to remove organic material, then dried at 90 °C for several hours. Once dry, 2.5-3.7 mg of each sample was weighed out, placed in partitioned glass tubes, reacted with phosphoric acid, and analyzed as described above. The amount of CO_2 produced from bulk samples was variable; each sample was analyzed one or two times, with each run consisting of 9-12 measurements, depending on the amount of CO_2 available for analysis.

Measured carbon and oxygen isotope values from all analyses were compared to the values expected from precipitation in isotopic equilibrium with DIC and water, respectively, using published fractionation factors for $CaCO_3$-HCO_3^- (Romanek et al. 1992) and $CaCO_3$-H_2O systems (Kim and O'Neil 1997, Coplen 2007, Wostbrock et al. 2020). Because $\delta^{17}O$ data for the water of Lake Fryxell are not presently available, expected $\delta^{17}O$ was calculated from $\delta^{18}O$ values assuming mass-dependent fractionation, using the equation:

$$\delta^{17}O = 0.528 \cdot \delta^{18}O \quad (1)$$

All isotopic data except for triple oxygen are presented here relative to the VPDB standard; some carbonate oxygen isotope data (including referenced published data) were recalculated to VPDB from VSMOW using the equation:

$$\delta^{x}O_{VPDB} = 0.97001 \cdot \delta^{x}O_{VSMOW} - 29.99‰ \quad (2)$$

where $\delta^{x}O$ represents the heavy oxygen isotope and X = 17 or 18. Triple oxygen data are presented relative to the VSMOW standard.

vii. Elemental Composition Analysis

Elemental composition data were acquired by laser ablation and inductively coupled plasma optical emission spectrometry (LA-ICP-OES). Elemental analysis focused on concentrations of Ca, Mn, and Fe; six standards were prepared by diluting BCS-CRM 393 limestone and NBS 2710 Montana soil with BCS-CRM 313 high-purity silica to create a set of references encompassing a range of Mn and Fe concentrations similar to the range expected in these samples (Table 4). After calculating the necessary proportions of each standard to achieve the desired Mn and Fe concentrations, the appropriate amount of each standard was measured out to bring each mixture to a total mass of 10±0.004 grams. The mixed standards were placed in SCP Science 33mm x 75mm polystyrene vials along with three SCP Science 11.0mm methyl methacrylate ball pestles in each vial and mechanically shaken for 5 minutes to homogenize. 8.85-9.05 g of each homogenized powder was mixed with 0.98-1.02 g of SCP Science SpectroBlend binding agent and homogenized again, following the same procedure. Homogenized powders were placed in foil trays and pressed into pucks with a Carver Auto Series NE hydraulic press using 25 tons of pressure for 2 minutes.

LA-ICP-OES was performed using a New Wave Research UP-213 laser ablation system connected to a PerkinElmer Optima 4300 DV optical emission spectrometer with Ar plasma and Ar as a carrier gas at a flow rate of 600 mL/min. Standards were measured first by designating a linear transect and ablating with the laser set to 80% power, a firing rate of 10 Hz, scanning speed of 8 μm/s, and a spot size of 55 μm. Standards were measured in

triplicate. The resulting peak intensities for Ca, Mn, and Fe were used to calculate calibration curves with which the intensities of each of these elements in samples could be quantified as concentrations in ppm. Ca, Mn, and Fe concentrations were measured at selected locations on billets corresponding to thin sections of carbonates from the samples designated Dredge1 B, LF 9.3 m, N-A.2, and LF 16Nov12 (see Table 2). All analyses were performed with the laser set to 80% power and 10 Hz firing speed, and one or two replicates were analyzed for each sampling site. Linear transects were scanned with a spot size of 55 or 80 μm and a scanning speed of 4-8 μm/s; single-spot analyses were performed with a spot size of 55-100 μm and a dwell time of 45-75 seconds. Analysis sites were selected based on CL and reflected-light images, focusing on areas of differing CL intensities (e.g. non-luminescent vs. bright, zones containing CL bands) and brown to black bodies identified as potential oxides of Fe and Mn entombed in carbonate.

IV. Results

i. Spatial Distribution of Carbonates

Carbonates are located in pore spaces in sediments and microbial mat biomass, but not at the mat-water/sediment-water interface. Carbonates are present throughout the lower oxycline and below the oxic-anoxic transition. Depth to carbonate from the mat-water/sediment-water interface ranges from 1-22 cm (Table 1). Depth to carbonate is independent of depth and microbial mat morphology.

ii. X-Ray Diffraction

XRD data show a spectral pattern characteristic of calcite, with a very strong peak around $2\theta = 30°$, three distinct peaks between $2\theta = 35\text{-}45°$, and a couplet of peaks near $2\theta = 50°$ (Figure 4) (Gunasekaran et al. 2006, Pesenti et al. 2008). XRD spectra are nearly identical at the upper and lower limits of the depth range (9.0 m and 9.7 m, respectively). Small amounts of quartz and feldspar are also evident on XRD spectra.

iii. Petrography

Lake Fryxell carbonates are found in close spatial association with sediments and microbial mat organic matter; sediment and mat biomass are typically observed surrounding and/or interspersed throughout carbonate-rich zones, commonly forming peloidal or thrombolitic fabrics (Figure 5, Figure 6). These mat-carbonate structures are not neatly laminated; instead, carbonates are present in irregularly-distributed pore spaces throughout mat biomass- and sediment-rich zones.

The most common petrographic texture observed in these samples is acicular crystals forming fan-like botryoidal structures, here referred to as “botryoids” (Figure 5A-C).

Individual botryoids are tens to hundreds of microns wide and hundreds of microns long in the direction of crystal growth. Acicular crystals also form isopachous cements composed of parallel crystals, which are less common than botryoids, but present in some deeper samples (Figure 5E). Discrete units of calcite crystals (i.e. botryoids or isopachous cements) adjacent to one another often grow in different directions rather than in a uniform orientation (Figure 5C, E). Botryoids exhibit sweeping extinction when rotated in cross-polarized transmitted light. Pointed needle-like crystal terminations characteristic of calcite are often visible in these cements. Blocky calcite is rare and only occurs near the edges of one sample from 9.6 m depth (Figure 5D).

Carbonates commonly exhibit multiple crystal growth directions at different locations within the same sample (Figure 6). Botryoids and isopachous cements most often grow outward from dark-colored areas indicative of high sediment and/or organic matter content (Figure 6). Carbonate crystals do not appear to preferentially grow in any specific direction in any of these samples.

iv. Cathodoluminescence

CL characteristics of Lake Fryxell carbonates vary across the oxycline transect. The CL observed in these carbonates is predominantly red, indicating coincident replacement of calcite Ca by both Mn and Fe (Hiatt and Pufahl 2014), and ranges from non-luminescent to bright (Figure 7). Small zones of green and blue CL are most likely due to crystal defects in the carbonates as well as minor amounts of quartz and feldspar, as indicated by XRD.

In shallower carbonates (9.0-9.3 m), discrete bands of bright red CL are common, typically appearing in concentric arrangements (Figure 8A-C). CL “bands” are visually

distinct, concentric or roughly parallel zones of carbonate alternating between dim to bright luminescence and non-luminescence and oriented approximately perpendicular to the crystal growth direction. Most of these bands are narrow (several microns wide) and very bright, although band width and intensity vary in some instances; bands can exhibit moderate to bright luminescence and rarely reach over 100 μm in width (e.g. Figure 8B). Dim and non-luminescent zones are nearly always significantly longer in the crystal growth direction than bright bands (Figure 8A-C).

In both shallow and deep samples, CL bands are present in both "clean" (little to no sediment/organic matter content) and "dirty" (high sediment/organic matter content) carbonate; bands in clean carbonate have well-defined edges and clear boundaries between luminescent and non-luminescent zones, while bands in dirty carbonate are often undulating (Figure 8A-C). Bands in clean carbonate can continue into zones of dirty carbonate, where they become more undulating and often less visually distinct from the surrounding carbonate (Figure 8B, Figure 9B). Dirty carbonate varies in CL intensity from non-luminescent to bright at shallower depths (9.0-9.3 m) and non-luminescent to dim in deeper samples (9.4-9.7 m) (Figure 8, Figure 9). In some occurrences, CL bands correspond to discoloration of the carbonate visible in transmitted light; discolored bands are light brown to nearly black (Figure 8E-F). However, most CL bands do not have this corresponding discoloration when viewed in transmitted light.

CL bands occur less frequently in deeper carbonates (9.4-9.7 m) than in shallower carbonates (9.0-9.3 m); approaching the oxic-anoxic transition depth (9.7 m), carbonates predominantly exhibit dim, diffuse CL or non-luminescence with rare narrow bands (Figure 9). Dim CL in deep samples is dim red to reddish-purple. Where bright bands are present,

they are very narrow (<10 μm in width) and flanked by wider zones of dim CL or non-luminescence (Figure 9B-C). Dim, diffuse red CL is more common than discrete bands and is typically surrounded by non-luminescent zones (Figure 9C).

v. Elemental Analysis

LA-ICP-OES reveals high variability in Mn and Fe concentrations in Lake Fryxell carbonates. Mn concentrations range from 44-8972 ppm, and Fe from 36-2182 ppm. The ratio of Fe to Mn also displays a broad range from 0.24-20.31. Ca concentrations were above the saturation limit of the instrument in nearly all sampling sites, and are not presented here.

Mn and Fe concentrations in these carbonates display a rough covariance; shallow (9.0 m) carbonate contains the lowest concentrations of both Mn and Fe, while the sampling sites with the highest Mn content also have the highest Fe content (Figure 10). The minimum concentrations of both Mn and Fe increase with depth. Concentrations of both metals vary widely at 9.3 and 9.7 m, with Mn concentrations ranging from 52-4173 ppm and Fe concentrations from 178-2418 ppm at these depths (Figure 11, Figure 12). The Fe/Mn ratio is <1 in 10 of 35 sample sites, with 7 of these sites containing dark brown to black spots surrounded by calcite. Two brown-to-black spots, one each at 9.3 and 9.4 m, yielded an Fe/Mn ratio >1. Dark brown to black spots identified in reflected-light images are present at each of the four depth points sampled by LA-ICP-OES.

In some sampling sites at 9.3 m, the Fe/Mn ratio corresponds to CL brightness across sets of CL bands; lower Fe/Mn is found in brighter zones and higher Fe/Mn in dimmer zones (Figure 13, Figure S5). However, Fe/Mn ratio does not correlate with CL intensity when the entire depth range is considered; most Fe/Mn ratios result in dim CL. These data do not make

evident a lower limit of Mn concentration required for CL activation, nor a specific Fe/Mn ratio required to extinguish CL.

vi. Manganese Oxides

Despite the near-zero DO concentration in the water column near the oxic-anoxic transition depth, Mn oxides can be found in carbonates from this depth. Identified by scanning electron microscopy and energy dispersive X-ray spectroscopy (SEM-EDS), these Mn oxides are roughly spherical, approximately 30 μm in diameter, and entombed in calcite (Figure 14, Figure S2). Mn and Fe oxides have been identified at this and shallower depths by LA-ICP-OES (see section IV, subsection iv).

vii. Stable Isotopes

Carbonate $\delta^{13}C$ follows an overall (but not uniform) increasing trend with depth, decreasing from 8.9 m to 9.3 m, then increasing below 9.3 m to a maximum at 9.7 m. Averages of measured values are similar to calculated equilibrium values in the mid-oxycline (8.9-9.0 m), but carbonate $\delta^{13}C$ becomes enriched relative to equilibrium values as depth increases, reaching +3.25‰ VPDB at 9.7 m (Figure 15).

Carbonate $\delta^{18}O$ in the lower oxycline is highly variable and does not follow a clear depletion or enrichment trend with depth (Figure 16). Carbonate $\delta^{18}O$ values exhibit a very broad range of over 20‰, and $\delta^{18}O$ does not co-vary with $\delta^{13}C$. In one sample from 9.3 m depth (LF 9.3 m), $\delta^{18}O$ values from drilling sites separated by microns to several millimeters are very heterogeneous, ranging from -26.4 to -3.09‰ VPDB (Figure 16, Figure S4). Neither $\delta^{13}C$ nor $\delta^{18}O$ correlate with redox conditions at the time of precipitation, as inferred from CL microscopy (Figure 16).

$\delta^{18}O$ values from triple oxygen isotope measurements exhibit significant variability, although the range of values is smaller than observed in the traditional $\delta^{13}C$ and $\delta^{18}O$ analysis; $\delta^{18}O$ from triple oxygen ranges from 1.8-8.2‰ VSMOW. $\delta^{18}O$ of bulk samples lies towards the lower end of this range, varying from 1.8-3.2‰, while drilled samples are more enriched in ^{18}O than bulk samples and are significantly different from each other (Table 5, Figure 17). The same relationship is true for $\delta^{17}O$; bulk samples range from 0.790-3.159‰ VSMOW, while drilled samples are more enriched and vary over a larger range (Table 5). All samples are depleted in ^{17}O relative to expected values calculated using Equation 1, with $\Delta^{17}O$ values ranging from -0.117 to -0.399‰ (Table 5). The slope between $\delta^{17}O$ and $\delta^{18}O$ is 0.526 ($R^2 = 0.995$), within the range of accepted values representing mass-dependent fractionation ratio between ^{17}O and ^{18}O (Figure 17). $\Delta'^{17}O$ does not covary with $\delta'^{18}O$ ($R^2 \approx 0$), and no oxygen isotope values show any trend with depth within Lake Fryxell.

V. Summary and Discussion

i. Summary

The microbial mat-associated carbonates found in the oxycline of Lake Fryxell provide a promising context in which to examine the preservation of local biogeochemical changes through space and time in a polar rock record, and to assess the relative importance of physical and biological contributions in a complex biogeochemical system. A number of biogeochemical factors including the stable density-based chemical stratification of the water column, infrequent disturbances to the lake, and abundant microbial communities in the lake benthos combine to create a range of markedly different biogeochemical environments in close proximity to one another, including substantial spatial and temporal changes in redox and biological activity influenced by the lake's perennial ice cover and the polar light-dark cycle. Carbonates in the benthic microbial mats of Lake Fryxell provide a local rock record which preserves petrographic and geochemical evidence of episodic precipitation which persisted for a period of multiple years. The data presented here describe a complex carbonate system whose spatial distribution, depositional timing, and redox and isotope geochemistry open several new avenues of study into modern and ancient perennially ice-covered lake deposits and their utility as proxies for perturbations in biogeochemistry and climate.

ii. Distribution of Lake Fryxell Carbonates

Prior to this study, the presence of microbial mat-associated carbonates in Lake Fryxell has been reported (Wharton et al. 1982), but little consideration has been given to the locations and timing of carbonate precipitation in this system. The petrographic data

presented here constitute the first such results from Lake Fryxell carbonates, and provide evidence for episodic carbonate precipitation inside microbial mat pore spaces.

Carbonates in Lake Fryxell are composed of calcite (Figure 4), predominantly as acicular crystals in fan-like botryoidal arrays or isopachous cements composed of parallel crystals. Carbonates are found in close association with microbial mat biomass, typically surrounded by and/or interspersed with peloidal clots of sediment and biomass (Figure 5). Crystal growth direction is non-uniform across the depth transect and within individual samples (Figure 6), indicating these carbonates nucleate within sediments and/or microbial mat surfaces and fill available pore spaces regardless of spatial orientation. Depth-to-carbonate measurements (Table 1) support this model of carbonate precipitation within pore spaces of microbial mats, as opposed to precipitation at the mat-water interface. Where carbonates lack incorporated sediment or microbial biomass, carbonates are interpreted to have precipitated within mm-scale voids. These spaces may form passively due to microbial mat growth processes, such as when microbial films overgrow open pits in ridge-pit mats (Jungblut et al. 2016), or when gas bubbles build up in mats and induce buoyant delamination of mat layers, a process which has been documented in photosynthetically active Lake Fryxell mats (Wharton et al. 1982, Wharton 1994). Such spaces provide abundant surface area within microbial mats on which carbonates nucleate with no preference for spatial orientation, resulting in a lack of uniform growth direction. This is in contrast to microbial mat-associated carbonate precipitation in Lake Joyce, Pearse Valley, MDV, where carbonates precipitate as crusts near the mat-water interface and grow outward at the surface of microbial mat structures (Mackey et al. 2015).

iii. Carbonate Precipitation Timing in Lake Fryxell

The presence of these carbonates as a single layer within microbial mat pore spaces is a useful indicator of precipitation as an episodic event rather than a constant background process, which would produce carbonate crusts at mat-water interfaces as has been documented in Lake Joyce (Mackey et al. 2015). The episodic nature of precipitation in Lake Fryxell is further supported by the presence of a correlative carbonate layer in two adjacent (~1.5 m apart) sand mounds on the lake bottom; the carbonate layer lies on top of one mound and at the bottom of the other (Rivera-Hernandez et al. 2019), indicating an episode of carbonate precipitation at some time between the deposition of the first and second sand mounds.

Cathodoluminescence (CL) microscopy images show that carbonate precipitation during episodic events in Lake Fryxell is continuous throughout changes in biogeochemistry over the course of the precipitation event. CL bands (Figure 8) indicate changes in Mn and Fe substitution in calcite during precipitation, and therefore changes in local redox, which can be attributed to the effects of the polar light-dark cycle on glacial melting and photosynthesis. Freeze concentration of gasses delivered by glacial melt streams is likely responsible for a large portion of summer DO input at the shallowest lake depths; Lake Hoare at the eastern end of Taylor Valley receives 89% of its DO from glacial melt water (Craig et al. 1992). During the austral summer, when sunlight is present 24 hours a day, glacial melt streams flow for several weeks and cyanobacteria in the mats can perform photosynthesis constantly, providing steady oxygen input and increasing DO over the course of the summer; DO is lowest at the beginning of summer, highest in mid-summer, and intermediate at the end of summer (Lawrence and Hendy 1985). During the constant

darkness of the austral winter, dissolved gas concentrations are predicted to increase at the bottom of the ice cover due to freeze concentration (e.g. Craig et al., 1992). At greater depths in the stratified water body, PAR declines to a level at which no photosynthesis can occur, leading to a reduction in oxygen with continuing respiration. This likely affects the depth of the oxic-anoxic transition within the density stratified water column; consistent oxygen input during summer would result in DO saturation to a greater depth, while the lack of oxygen input in winter would shift the oxic-anoxic boundary to a shallower depth. Vertical movement of the oxycline has not been directly observed in Lake Fryxell to date, but can be reasonably assumed from previous observations of seasonal changes in DO at the oxycline (Lawrence and Hendy 1985). The extent of the oxycline's movement appears to be variable from year to year; lower abundance of bright CL bands at 9.0 m (Figure 8A) indicates this depth rarely experiences redox conditions reducing enough to allow Mn/Fe substitution in calcite, while the abundance of bands at 9.3 m (Figure 8B,C) documents frequent and significant changes in redox at this depth, potentially an annual cycle resulting from movement of the oxycline across this depth and fluctuation in microbial photosynthesis.

From these petrographic and CL observations, it can be inferred that carbonate precipitation in Lake Fryxell is not controlled by seasonal fluctuations in biogeochemistry, but occurred as a discrete event that persisted through multiple annual light-dark cycles and associated changes in pore water redox.

iv. Redox Geochemistry of Lake Fryxell Carbonates

LA-ICP-OES analysis focused on carbonate Mn and Fe content reveals a complex redox system in the oxycline of Lake Fryxell. Mn and Fe content of carbonates varies widely

across the oxycline and within individual samples (Figure 10), with concentrations of both metals ranging from tens to thousands of ppm. Mn and Fe concentrations in carbonates follow a rough increasing trend with depth (Figure 10); carbonate from 9.0 m, where both Mn and Fe concentrations are near their lowest (Harnish et al. 1991) has near-zero Mn and Fe concentrations, while deeper carbonates display higher concentrations of both metals (Figure 10, Figure 11, Figure 12). However, carbonate Mn and Fe concentrations at depths below 9.0 m are variable over broad ranges (Figure 11, Figure 12) and do not display a clear correlation to water column concentrations, indicating these carbonates do not incorporate Mn and Fe from the water column based solely on the amount of each metal available. For the purposes of interpreting these data, Mn and Fe water column concentrations from Harnish et al. (1991) were correlated to the sampling depths in 2012 based on the depth of the oxic-anoxic transition.

Because Lake Fryxell carbonates form within microbial mat pore spaces, the role of biology in the geochemistry of these carbonates must be taken into account, particularly when redox is considered. Photosynthesis in the mats directly affects pore water redox via oxygen production, which can create oxidizing microenvironments within microbial mats; elevated oxygen concentrations in mats relative to the water column have been documented at both oxic and anoxic depths in Lake Fryxell (Sumner et al. 2015). Where these pore waters are sufficiently oxidizing, Mn and Fe can be sequestered into insoluble oxide phases, preventing substitution into carbonates. The presence of Mn-bearing oxides (identified as dark brown to black spots displaying high Mn concentrations) in carbonates at two of the four depths sampled by LA-ICP-OES (Figure 10) indicates the role of these oxidizing microenvironments on Mn and Fe redox in pore waters; oxidized Mn (Mn^{3+}/Mn^{4+}) is

thermodynamically unstable in aqueous environments unless conditions are strongly oxidizing (Davison 1993), and the water column at the depths at which Mn-bearing oxides are present (9.3 and 9.7 m) are slightly below oxygen saturation to anoxic (Dillon et al. 2020a), thus necessitating the formation of these oxides within a more oxidizing microenvironment. Mn oxides may also be formed via microbial enzymatic processes (Nealson 2006, Sutherland et al. 2017), however no Mn-oxidizing organisms have been identified in Lake Fryxell at this time, implicating photosynthetic oxygenation of pore waters as the primary mechanism for Mn oxide formation.

Together, CL imaging and LA-ICP-OES analysis of these carbonates describe a complex redox system. CL bands provide a record of seasonal changes in pore water redox which correspond well to fluctuations in the carbonate Mn and Fe concentrations in instances where bands can be accurately sampled by laser ablation, such as in a set of bands at 9.3 m where the influence of Fe/Mn ratio on CL brightness is readily apparent (Figure 13). However, the relationship between CL and Fe/Mn concentrations is not consistent throughout all carbonates in the oxycline; CL brightness appears independent of metal concentrations in the majority of LA-ICP-OES sampling sites (Figure 10). This may be due in part to the non-selective nature of LA-ICP-OES; laser ablation does not differentiate between redox states, instead capturing all Mn and Fe present in the carbonate regardless of oxidation state. Since only reduced Mn and Fe affect carbonate CL, ablation of oxidized Mn and Fe may complicate interpretation of these data. Thus, careful interpretation of combined petrographic, CL, and LA-ICP-OES data sets is necessary to accurately assess carbonate redox geochemistry and the seasonal changes therein.

From the combination of CL imaging and geochemical data, it can be inferred that rather than directly recording water column metal concentrations, carbonate redox geochemistry in Lake Fryxell preserves a record of seasonal changes of the oxic-anoxic transition depth and pore water oxygenation, most likely resulting from the changing availability of solar radiation throughout the polar light-dark cycle. Both Mn and Fe concentrations show the broadest range at a depth of 9.3 m (Figure 11, Figure 12), providing a geochemical record of the frequent changes in redox evident from the abundant CL bands at the same depth. This implicates 9.3 m as a depth across which the oxic-anoxic boundary regularly moves; as oxygenation of the water column and pore waters changes seasonally, redox at 9.3 m changes to enable or prevent substitution of reduced Mn and Fe into calcite, resulting in both abundant CL band formation and variable Mn and Fe content of carbonates at this depth. In contrast, CL bands in carbonates at 9.0 m are less abundant and much narrower than bands at 9.3 m, indicating that pore waters at this depth typically remain oxygenated perennially and are rarely reducing enough to allow Mn/Fe substitution into carbonates.

From the petrographic and redox-based observations presented here, it is apparent that carbonate precipitation in Lake Fryxell is an episodic process which can proceed continuously over the course of multiple annual light-dark cycles and capture seasonal fluctuations in pore water redox, most likely caused by a combination of vertical movement of the oxic-anoxic transition zone and seasonal changes in glacial melt and microbial metabolism with PAR availability. Microbial photosynthesis is an important factor in the redox geochemistry of these carbonates via its influence on pore water oxygenation, but does

not appear to control precipitation timing, as these carbonates precipitate through significant changes in redox.

v. Isotope Geochemistry of Lake Fryxell Carbonates

Carbon isotopes of Lake Fryxell carbonates provide a signature of metabolic activity via enrichment in ^{13}C. $\delta^{13}C$ is slightly enriched (~2-3.25‰ VPDB) at the majority of points sampled (17 of 22 sampling sites) (Figure 16) and is enriched relative to values predicted by calculations for precipitation in isotopic equilibrium with the water column (after Romanek et al. 1992) (Figure 15), consistent with preferential uptake of ^{12}C by photosynthesis. Microbial photosynthesis removes ^{12}C from the DIC pool, leaving a more enriched carbon pool from which carbonates can precipitate, ultimately resulting in these carbonates becoming more enriched in ^{13}C. However, the carbon isotope signature in these carbonates does not appear to record seasonal fluctuations in metabolic activity; $\delta^{13}C$ does not show any covariance with the changes in redox evident from CL imaging, nor is there a uniform trend in $\delta^{13}C$ with depth (Figure 16). Therefore, carbonate $\delta^{13}C$ cannot be used to assess seasonal changes in microbial metabolism at the sampling resolution carried out in this study.

The wide range of approximately 24‰ in $\delta^{18}O$ of Lake Fryxell carbonates is unusual. The water column of Lake Fryxell is isotopically light in oxygen (average $\delta^{18}O \approx$ -31.6‰ VSMOW or -60.6‰ VPDB) and nearly uniform with respect to $\delta^{18}O$; across 10 meters of depth, $\delta^{18}O_{water}$ varies over a range of <1‰ (Dowling and Lyons 2014). At present, no $\delta^{18}O$ data exist for DIC in Lake Fryxell; however, isotopic equilibrium between DIC and water is assumed, as equilibration between DIC and water is achieved within hours to days

(Wostbrock and Sharp 2021 and references therein). Equilibrium fractionation calculations predict carbonate $\delta^{18}O$ values of -27.5‰ to -25.6‰ VPDB (2.6-4.5‰ VSMOW) at all depths in the lower oxycline (after Kim and O'Neil 1997, Coplen 2007, Wostbrock et al. 2020). The cause of this offset and variability in carbonate $\delta^{18}O$ is unclear at present. Sampling sites only millimeters apart exhibit large (up to 22‰ in sample LF 9.3) differences in $\delta^{18}O$ (Figure S4). In contrast to Lake Fryxell carbonates, $\delta^{18}O$ values of carbonates from stromatolites in Lake Joyce vary over only 5.5‰ and do not exhibit such broad variability on the μm-to-mm scale (Mackey et al. 2018). Thus, the oxygen isotope composition of Lake Fryxell carbonates must be influenced by some process which does not occur in Lake Joyce.

A number of kinetic effects have been found to enhance ^{18}O fractionation in carbonate-water systems; fractionation is greater at low temperatures, circumneutral pH, and when precipitation rates are very slow (Dietzel et al. 2009, Gabitov et al. 2012). Additionally, low temperatures may slow the activity of the enzyme carbonic anhydrase, which is found in cyanobacteria and promotes ^{18}O equilibration between carbonates and DIC (Uchikawa and Zeebe 2012, Watkins et al. 2013). However, the triple oxygen isotope composition of these carbonates indicates mass-dependent fractionation rather than kinetic fractionation. The $\delta^{17}O/\delta^{18}O$ slope of 0.526 is well within the range of accepted values for mass-dependent oxygen isotope fractionation (Wostbrock et al. 2020, Wostbrock and Sharp 2021), and as such indicates no significant influence of kinetic effects on the oxygen isotope composition of these carbonates. Rather, the oxygen isotope variability of Lake Fryxell carbonates may be indicative of isotopic heterogeneity in the fluid from which these carbonates precipitated, caused by mixing of multiple water sources with significantly different oxygen isotope compositions.

Glacial melt streams and shallow groundwater in the Fryxell basin are slightly heavier (0.8-1.2‰) in ^{18}O than the water column of Lake Fryxell (Gooseff et al. 2006, Harris et al. 2007), but this relative enrichment is not of a sufficient magnitude to explain the oxygen isotope offset observed in Lake Fryxell carbonates (Figure 19), indicating that mixing with these waters may contribute to carbonate ^{18}O enrichment, but is not the sole cause of the isotopic offset in these carbonates. Triple oxygen isotope compositions of Lake Fryxell carbonates may help to further constrain the possible source fluids which putatively cause this disequilibrium. While ^{3}H enrichment of deep waters in Lake Fryxell indicates some infiltration of freeze-concentrated meteoric waters into the stratified water body (Miller and Aiken 1996), unmodified meteoric waters are not a plausible mechanism for the $\delta^{18}O$ offset of Lake Fryxell carbonates, as precipitation in equilibrium with meteoric waters would yield carbonate $\Delta'^{17}O$ values around 0‰ VSMOW (Sharp et al. 2018), 0.15-0.4‰ higher than the values observed in these carbonates (Figure 18). In addition, freeze-concentrated waters would have lower $\delta^{18}O$ values than their source fluids (e.g. Horita 2009), and therefore would not cause the ^{18}O offset observed in these carbonates. Evaporatively-enriched marine waters are a plausible source fluid; $\Delta'^{17}O/\delta'^{18}O$ of these carbonates (Figure 18) falls well below fractionation curves for calcite precipitation in equilibrium with modern seawater at temperatures near 0 °C (Wostbrock and Sharp 2021), indicating that any marine waters infiltrating into the lake have been modified from their original isotopic composition. Thus, under this fluid-mixing hypothesis, a water source must be invoked which is not glacial or meteoric in origin, but may be a modified marine water resulting from evaporative ^{18}O enrichment of paleolake waters and/or melting of buried ^{18}O-enriched ice remaining from the advance of the Ross Ice Sheet during the LGM.

Lake Fryxell is connected via a talik (an unfrozen region of ground bounded by permafrost) to a calcium chloride-rich subsurface brine aquifer which connects to the ocean at the McMurdo Sound approximately 5 km away from the lake (Figure S3) (Toner and Sletten 2013, Mikucki et al. 2015, Foley et al. 2019). This aquifer is putatively a remnant of a paleolake, Glacial Lake Washburn, which infiltrated the ground after freezing and/or evaporation created a concentrated brine (Mikucki et al. 2015, Myers et al. 2021). It is possible that this brine episodically infiltrates through the lake floor at specific points and mixes with the pore waters from which carbonates precipitate. This infiltration may be spatially non-uniform due to heterogeneity in soil permeability and porosity, which could contribute to spatial variation in carbonate $\delta^{18}O$ if the brine and lake waters differ in their isotopic compositions. This brine would likely be enriched in ^{18}O due to evaporative concentration. However, evaporation of meteoric waters alone can not fully explain the range of carbonate $\delta^{18}O$ seen here; Don Juan Pond, a shallow hypersaline brine pond located in Wright Valley, MDV, is highly evaporatively concentrated and appears to represent the upper limit of evaporative ^{18}O enrichment of meteoric waters in the MDV, with $\delta^{18}O_{water}$ values up to -8.3‰ VSMOW (Matsubaya et al. 1979, Horita 2009). The $\delta^{18}O$ values of this water would not yield the highest calcite $\delta^{18}O$ values presented here (Figure 19), and as such evaporation of meteoric waters alone can not be the sole mechanism responsible for the $\delta^{18}O$ offset in Lake Fryxell carbonates; instead, a marine influence must be invoked, as seawater is isotopically heavier than the other water sources available in the MDV (Figure 19). Lawrence and Hendy (1989) suggested precipitation from seawater as a possible explanation for ^{18}O enrichment of carbonates in earlier sediments deposited from Glacial Lake Washburn.

Modern seawater in the Southern Ocean is more enriched in ^{18}O than the lacustrine, glacial, and meteoric waters in Taylor Valley (Srivastava et al. 2007), and was further enriched during the LGM (Lea et al. 2002). Thus, it is plausible that a marine-influenced water mixes with Lake Fryxell waters and increases $\delta^{18}O$ of pore waters, subsequently increasing carbonate $\delta^{18}O$. Seawater has previously been hypothesized as a source water for ^{18}O-enriched carbonates in Lake Fryxell sediments (Lawrence and Hendy 1989), but the mechanism by which seawater may enter Lake Fryxell has yet to be determined. The reservoir may be the ocean itself, since the brine aquifer connects Lake Fryxell to the McMurdo Sound (Mikucki et al. 2015), or buried ice remaining from the Last Glacial Maximum. Airborne electromagnetic surveying (AEM) of the Fryxell basin has revealed sub-surface ice within hundreds of meters to kilometers of Lake Fryxell (Mikucki et al. 2015, Myers et al. 2021). This ice most likely represents remnants of grounded ice which advanced from the Ross Sea embayment during the LGM (Christ and Bierman 2020, Myers et al. 2021). Because freezing of water produces ice enriched in ^{18}O relative to the source water (e.g. Horita 2009), this buried ice could be enriched in ^{18}O relative to other water sources in Taylor Valley. Thus, modified seawater and buried ice are hypothesized to have been sources of water with enriched $\delta^{18}O$ values which may have contributed to the ^{18}O enrichment and variability of these carbonates. Changes in regional hydrology with warming regional climate may have caused either local melt of ground ice or reflux of subsurface fluids. These fluids would have flowed through the subsurface and infiltrated into the sediments and microbial mat pore spaces in Lake Fryxell, causing a perturbation to the geochemistry of these pore waters and inducing carbonate precipitation.

These oxygen isotope data open new avenues of research into the geochemistry of Antarctic carbonates and waters. At present, no oxygen isotope data exist for the brine aquifer or buried ice around Lake Fryxell, so it is as yet indeterminate whether infiltration of these waters would result in the oxygen isotope offset observed in these carbonates. Additionally, the high variability of $\delta^{18}O$ across μm to mm in Lake Fryxell carbonates highlights the importance of high-resolution sampling in carbonate isotope analysis; bulk analysis obscures this variability and may bias interpretation if fine-scale sampling is not performed. Ultimately, further study of the isotope chemistry of water sources in the Fryxell basin and in other areas of the MDV is needed to elucidate the mechanism(s) responsible for the oxygen isotope phenomena observed in Lake Fryxell carbonates, as well as the potential processes which induce carbonate precipitation in the MDV lakes.

VI. Conclusions

Microbial mat-associated carbonates in Lake Fryxell provide a sedimentary record of episodic carbonate precipitation across depth-based biogeochemical gradients and through temporal changes in redox. CL imaging shows that episodic precipitation events in Lake Fryxell can persist for multiple years, with precipitation continuing through seasonal changes in pore water redox as microbial photosynthetic activity and the oxic-anoxic transition depth fluctuate through the annual light-dark cycle. Carbonate Mn/Fe content further indicates variability of local redox in microbial mat pore spaces, both with depth as the lake transitions from oxygen supersaturation to anoxia and seasonally over the course of the polar light-dark cycle. Both $\delta^{13}C$ and $\delta^{18}O$ in these carbonates are inconsistent with predictions for precipitation in isotopic equilibrium with the water column. Carbonate $\delta^{13}C$ shows overall enrichment relative to predicted equilibrium values, consistent with preferential uptake of ^{12}C by metabolic processes, but does not covary with precipitation timing or redox. Carbonate $\delta^{18}O$ is offset from expected values for precipitation in equilibrium with the water column, and is highly variable on very small spatial scales, likely indicating mixing of multiple water sources during carbonate precipitation. As indicated by previous ^{18}O data collected from Taylor Valley and the carbonate triple oxygen isotope data presented here, these waters are not glacial or meteoric in origin and may originate from evaporatively concentrated subsurface brine, modified seawater, and/or buried ice remaining from the Last Glacial Maximum; further study of the hydrology and isotopic compositions of different waters in the Fryxell basin is necessary to address these carbonate oxygen isotope phenomena.

In summary, the findings presented here lead to the following conclusions on carbonate precipitation timing and geochemistry in the oxycline of Lake Fryxell:

1) Calcite precipitates as acicular botryoidal and isopachous cements within pore spaces in microbial mats. Precipitation is episodic, and precipitation events can last for multiple years, with consistent precipitation through seasonal changes in redox.
2) Microbial metabolism influences the redox geochemistry of carbonates precipitating in mat pore spaces, but does not control the timing of precipitation.
3) Carbonate $\delta^{13}C$ is enriched relative to expected values for precipitation in equilibrium with DIC, consistent with preferential uptake of ^{12}C by microbial metabolism. $\delta^{13}C$ does not covary with carbonate redox, suggesting no significant difference in the effects of microbial photosynthesis and respiration on carbonate $\delta^{13}C$ at the level of resolution employed in this study.
4) Carbonate $\delta^{18}O$ is enriched relative to calculated equilibrium precipitation values, is highly variable over small (μm to cm) distances, and does not covary with depth or redox, suggesting mixing of multiple isotopically heterogeneous waters in the benthic zone of the lake.
5) Triple oxygen isotopes of these carbonates suggest mixing with evaporatively-concentrated waters and/or marine-influenced waters, which may infiltrate through lake sediments from a subsurface brine aquifer and/or as meltwater from buried ice remaining from the Last Glacial Maximum.

The petrographic and geochemical observations presented here indicate that while these carbonates precipitate in close proximity to metabolically active microbes, and that microbial metabolism influences the geochemistry of these carbonates, biological activity is not a controlling factor in precipitation timing. Rather, isotopic evidence points towards a

perturbation to the local climate as the primary driver of carbonate precipitation in Lake Fryxell. Formation of brines by evaporative concentration or melting of buried relict ice triggered by post-LGM warming likely introduced foreign waters to Lake Fryxell whose chemistry differs from the lake waters, disrupting the carbonate equilibrium in pore waters and inducing carbonate precipitation.

The observations presented here constitute the first petrographic and geochemical investigation of Lake Fryxell carbonates, as well as the first triple oxygen isotope analysis of Antarctic carbonates. Altogether, these data provide a set of petrographic and geochemical proxies applicable to analysis of modern Antarctic carbonates as well as Antarctic paleolake deposits, such as the microbial mat-associated carbonates in Lake Joyce and the paleolake carbonates remaining from Glacial Lake Trowbridge in Miers Valley, MDV (Clayton-Greene et al. 1988), and to interpretation of the role of climate perturbations in the deposition of such carbonates. Further study is needed to more accurately constrain the drivers of Antarctic lacustrine carbonate precipitation and biogeochemical factors influencing the geochemistry of such carbonates; at present, no redox data exist for carbonates from other MDV lakes, and high-resolution carbonate isotope data have been collected from only one other MDV lake, Lake Joyce. Investigation of the redox and isotope geochemistry of both modern lacustrine carbonates and paleolake deposits in the MDV will expand our understanding of climate change in polar environments and the capabilities of lacustrine carbonates to record these changes.

Table 1. Measurements of depth to carbonate from the microbial mat-water interface. Depth to carbonate is variable and shows no relation to depth or mat texture. N/A = not recorded.

Site Depth (m)	Depth to Carbonate (cm)	Mat Texture
9.3	2	Sand mound
9.4	22	Sand mound
9.4	2	Ridge-pit mat
9.5	12	Pinnacles in ridge-pit mat
9.5	4	Ridge-pit mat
9.8	14	Small sand mound
9.8	2	Prostrate mat
9.8	4	Prostrate mat
9.9	2	N/A
9.9	1	Knobs
9.9	12	Sand mound
10.2	1.6	N/A
10.2	1.6	N/A
10.2	6	N/A
N/A	2	Knob in ridge-pit mat

Table 2. Designations and descriptions of samples selected for use in this study. See Jungblut et al. (2016) for details of microbial mat morphologies. Dissolved oxygen data from Jungblut et al. (2016). N/A = not recorded.

Sample	Depth	DO (mg/l)	Description
Dredge1 A	9.0 m	15.2	Carbonate from pitted pinnacle mats
Dredge1 B	9.0 m	15.2	Carbonate from pitted pinnacle mats
LF 9.3 m	9.3 m	7.4	Carbonate from pinnacle mats
N-A.2	9.4 m	4.5	“Knob” structure in ridge-pit mat
J.2-A	9.6 m	N/A	Carbonate from mat overlying sand mound
LF 9.7 m	9.7 m	0.2	Carbonate from ridge-pit mats
LF 16Nov12	9.7 m	0.2	Carbonate from ridge-pit mats

Table 3. Accepted $\delta^{13}C$ and $\delta^{18}O$ values for the isotopic standards used in this study. All values are reported on the VPDB scale. Standard composition values obtained from the International Atomic Energy Agency (IAEA).

Standard	$\delta^{13}C$ (VPDB)	$\delta^{18}O$ (VPDB)
NBS-19	+1.95‰	-2.20‰
IAEA CO-8	-5.764‰	-22.7‰
IAEA CO-9	-47.321‰	-15.6‰
Carrara Marble (IAEA 603)	+2.46‰	-2.37‰

Table 4. ICP-OES standard compositions and Fe and Mn concentrations. Concentrations are given in ppm. (Note: Standard #1 was discarded due to low mass and issues during the pressing process).

Std. #	Composition	[Fe]	[Mn]
2	100% BCS-CRM 393	450	100
3	50% BCS-CRM 313, 50% BCS-CRM 393	284.9	50.6
4	90% BCS-CRM 313, 10% BCS-CRM 393	153.0	11.2
5	97% BCS-CRM 313, 3% NBS 2710	1130.1	304.2
6	98% BCS-CRM 313, 2% NBS 2710	796.3	204.1
7	95% BCS-CRM 313, 5% NBS 2710	1803.3	506.0

Table 5. $\delta^{18}O$, $\delta^{17}O$, and $\Delta^{17}O$ values of Lake Fryxell calcite. All data are presented as permille values relative to the VSMOW standard. Values are averages of 9 to 12 measurements per analysis. Samples with identical names indicate replicate analyses of CO_2 produced from the same sample.

Sample	$\delta^{18}O_{calcite}$	$\delta^{17}O_{calcite}$	$\Delta^{17}O_{calcite}$	Depth (m)	Preparation
Dredge1 bulk #2	2.3771	0.8542	-0.1639	9.0	Bulk
Dredge1 bulk #3	3.1548	1.4922	-0.1172	9.0	Bulk
N-A.2 #2	3.4169	1.5837	-0.2186	9.4	Drilled
N-A.2 bulk #2	1.8371	0.7901	-0.2188	9.4	Bulk
N-A.2 bulk #2	2.0966	0.9297	-0.1515	9.4	Bulk
N-B.1 bulk #1	3.0453	1.3922	-0.1917	9.4	Bulk
N-B.1 bulk #1	3.0784	1.4244	-0.3997	9.4	Bulk
J.2-A bulk #2	2.8193	1.3359	-0.2089	9.6	Bulk
J.2-A bulk #2	2.7017	1.2336	-0.1720	9.6	Bulk
J.2-A bulk #3	3.1598	1.5030	-0.1639	9.6	Bulk
16Nov12 #3	8.2316	4.1181	-0.2188	9.7	Drilled
16Nov12 #2	5.8481	2.8740	-0.2089	9.7	Drilled

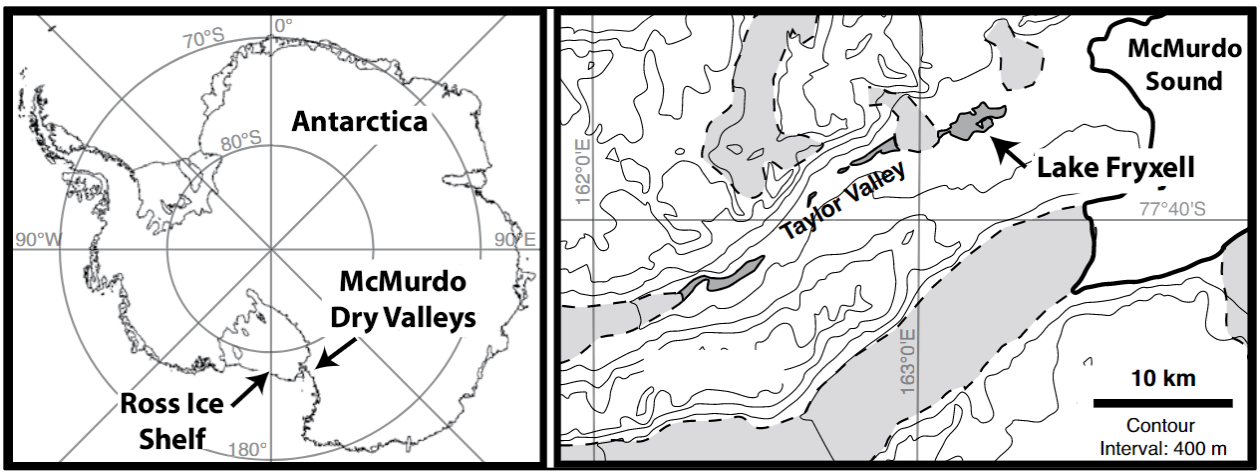

Figure 1. Location of the McMurdo Dry Valleys and Ross Ice Shelf in Antarctica, and location of Lake Fryxell in Taylor Valley (adapted from Sumner et al. 2015).

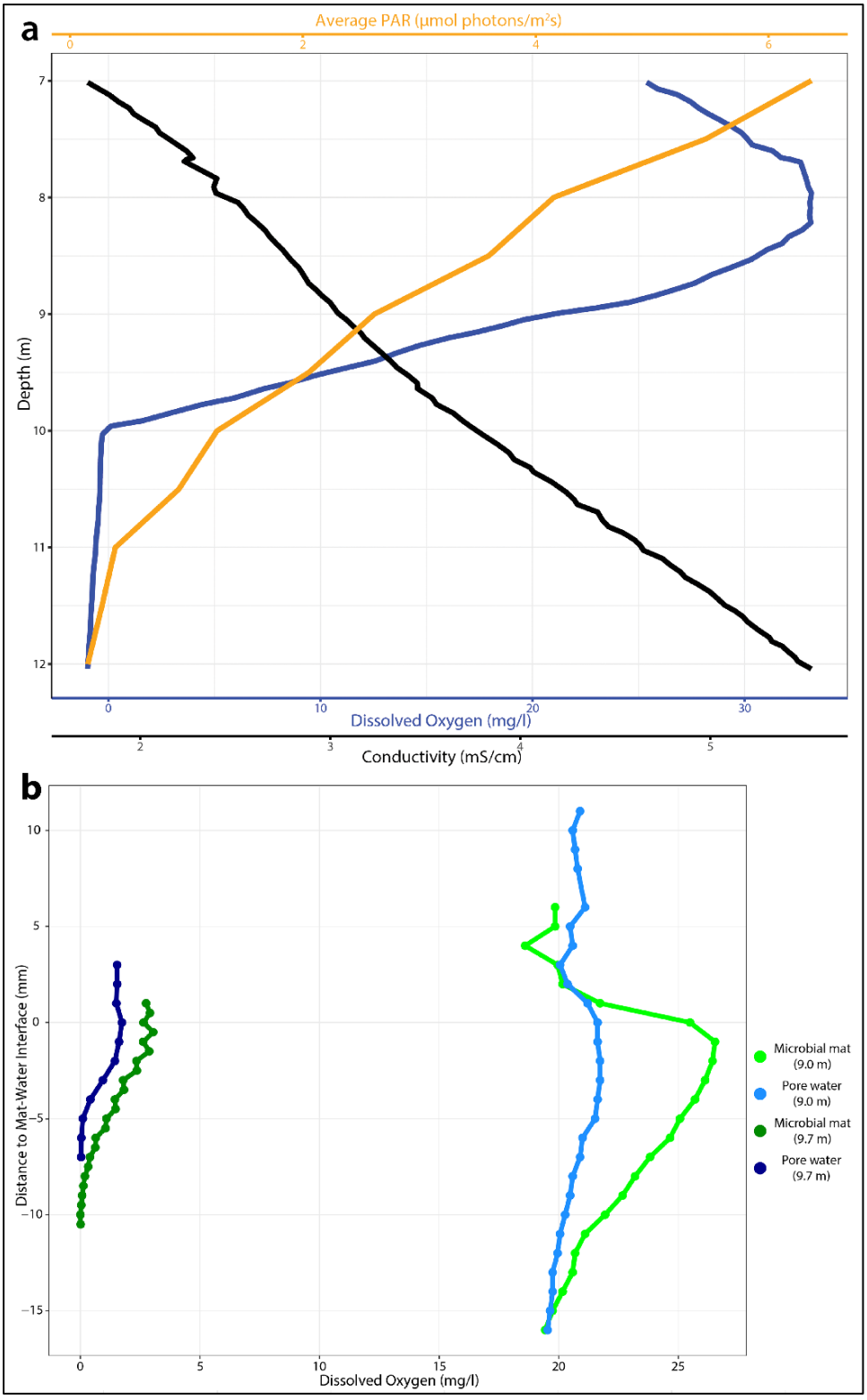

Figure 2. (A) The DO maximum occurs around 8 m depth in Lake Fryxell, below which is a steep oxycline. DO disappears from the water column by 10 m. PAR is low due to attenuation of sunlight by the ice cover and decreases with depth. Conductivity increases with depth due to stratification and lack of mixing (adapted from Dillon et al. 2020a). (B) Microelectrode profiles across the mat-water interface show elevated oxygenation in microbial mats (adapted from Sumner et al. 2015).

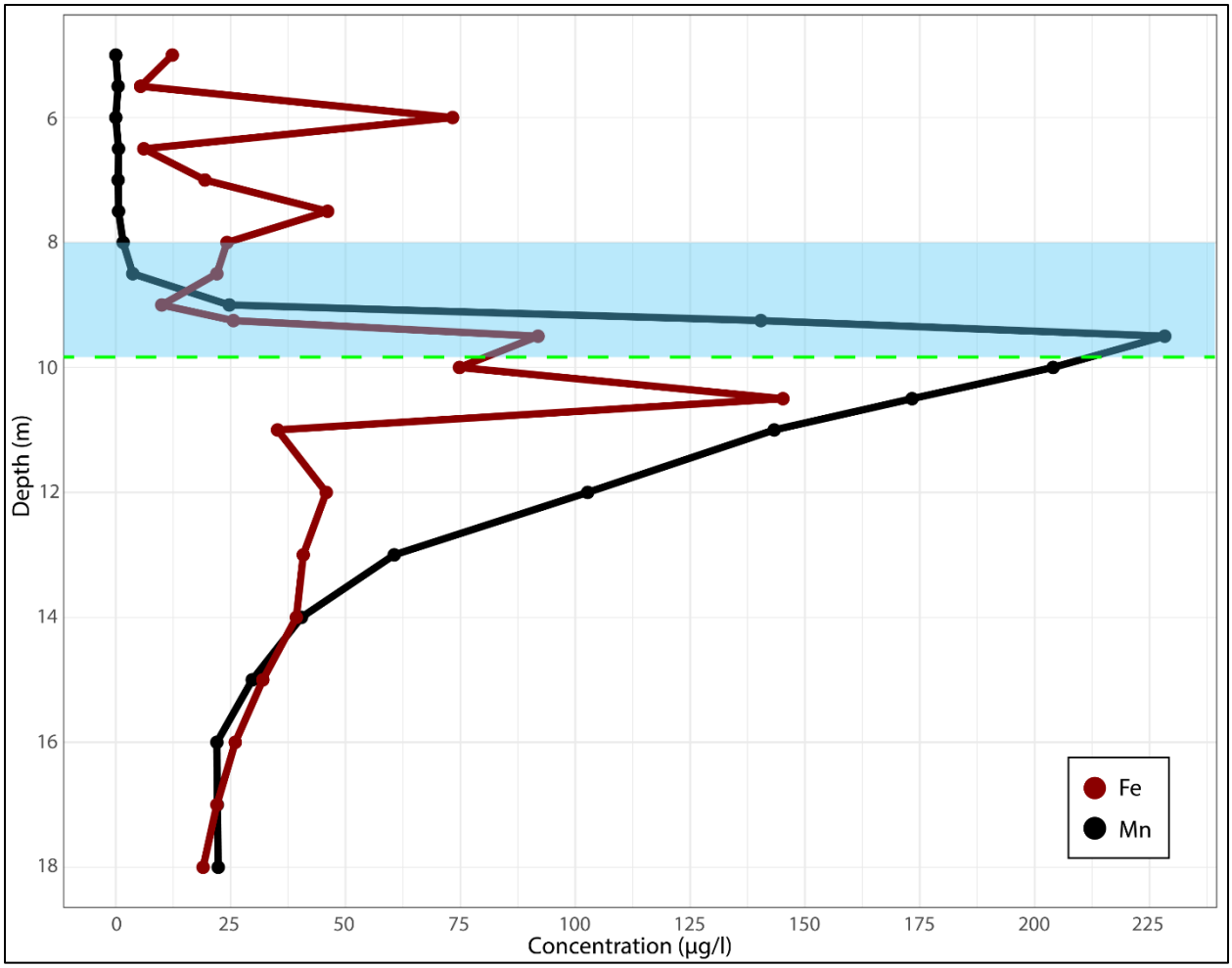

Figure 3. Total Mn and Fe concentrations in the water column of Lake Fryxell, including dissolved (<100,000 Da), colloidal (100,000 Da to 0.45 µm), and particulate (>0.45 µm) phases of both metals. Maximum concentrations of both Mn and Fe are located near the oxic-anoxic transition depth, with low concentrations at shallower oxic depths likely due to formation of insoluble oxides. The depth range comprising the oxycline is shaded blue, and the oxic-anoxic transition depth is represented by the dashed green line (adapted from Harnish et al. 1991).

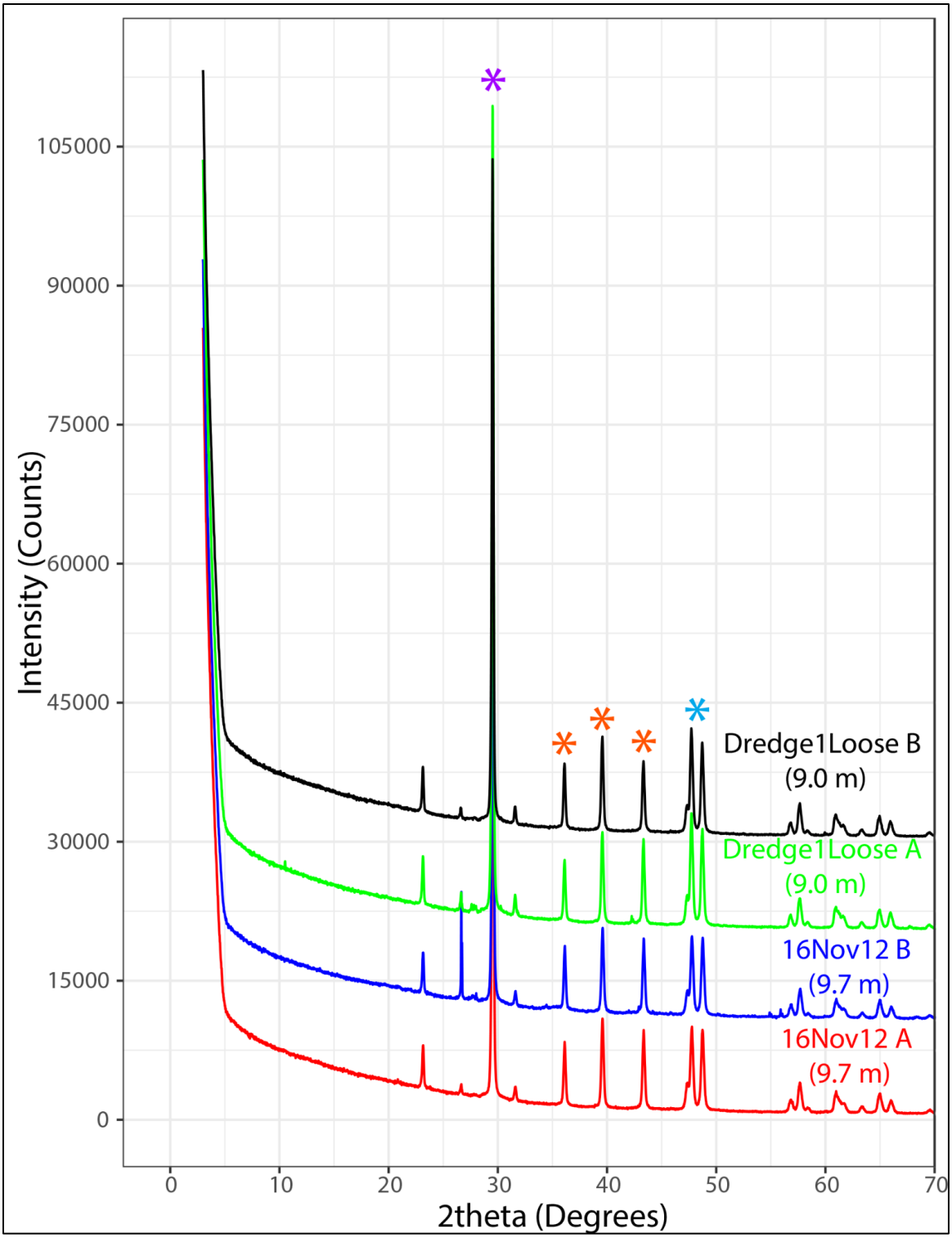

Figure 4. XRD spectra from four carbonate samples taken from the upper and lower limits of the depth transect considered in this study. Spectral patterns show these carbonates consist almost entirely of calcite, as indicated by the strong peak around 2θ = 30° (purple star), three medium-size peaks between 2θ = 35-45° (orange stars), and couplet near 2θ = 50° (cyan star).

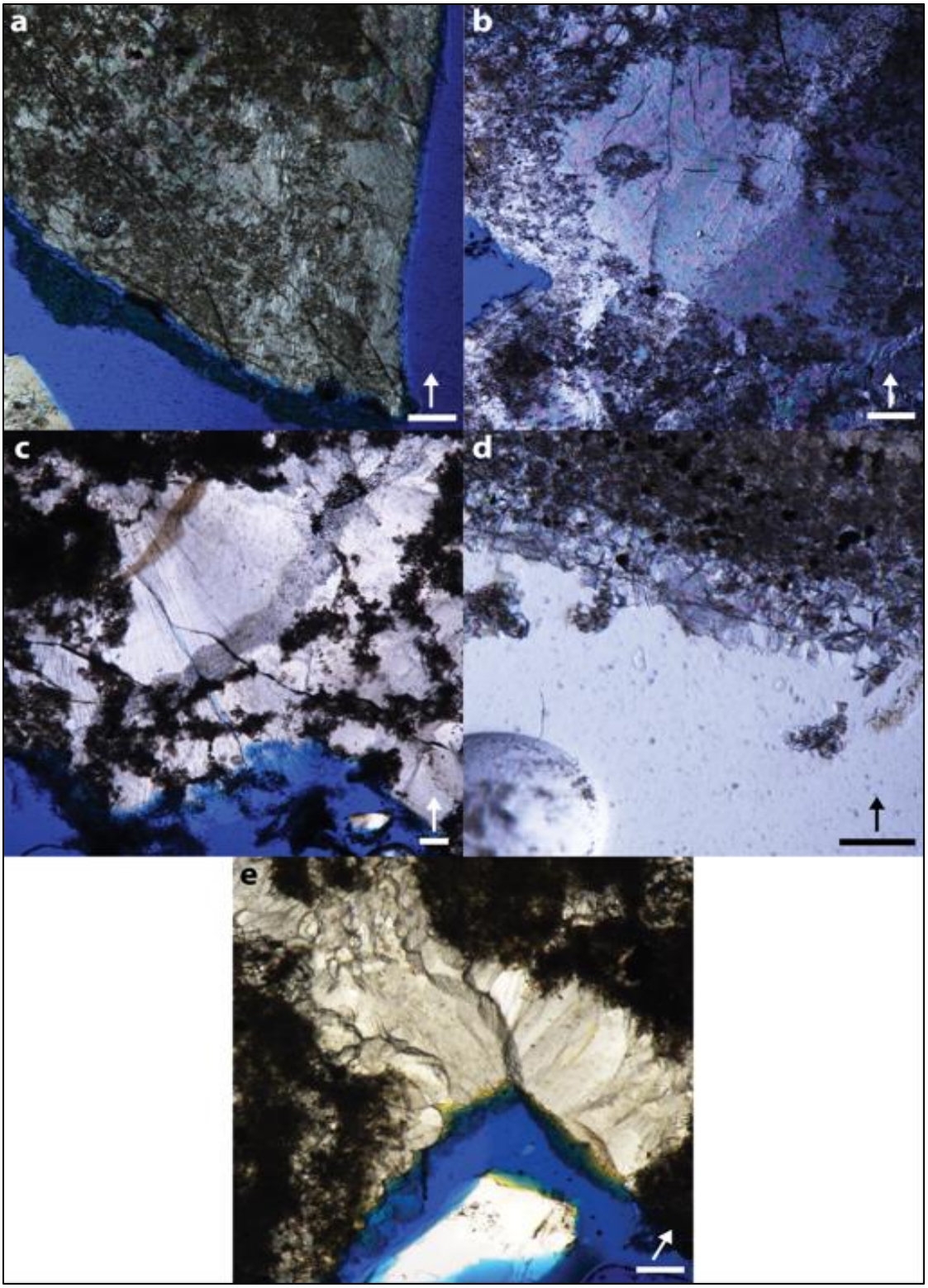

Figure 5 (previous page). Plane-polarized transmitted-light photographs showing major petrographic textures in Lake Fryxell carbonates. Acicular botryoids are the most common texture, shown here at 9.0 m (A-B) and 9.3 m (C). Blocky calcite is rare, but present at 9.6 m (D). Acicular isopachous cements occur near the oxic-anoxic transition; distinct groups of crystals grow in different directions (E). Arrows indicate direction to mat-water interface. Scale bars are 100 μm.

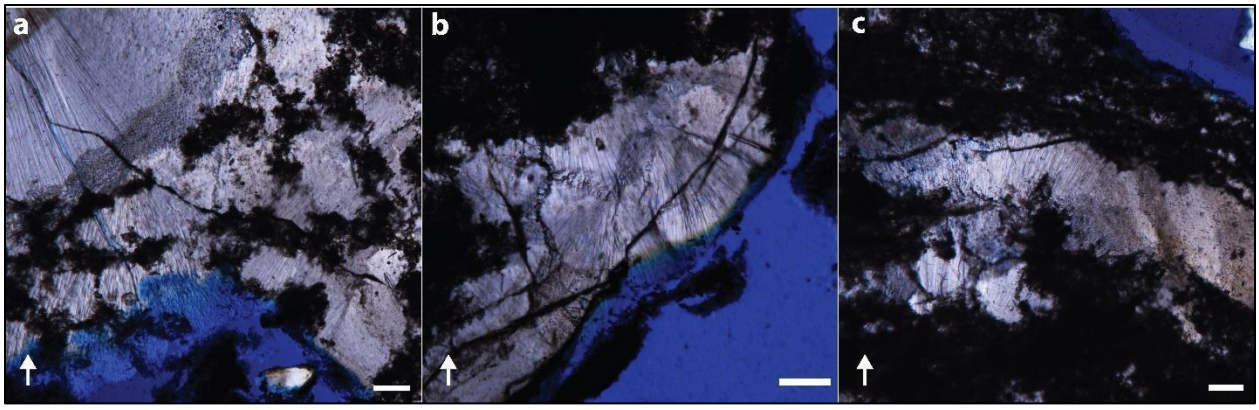

Figure 6. Plane-polarized transmitted-light photographs showing acicular botryoids growing in non-uniform orientations within the same sample (LF 9.3 m). Growth direction differs over distances of tens to hundreds of microns in adjacent botryoids (A-B). Botryoids appear to nucleate in sediments/mat biomass and fill pore spaces (C). Arrows indicate direction to the mat-water interface. Scale bars are 100 μm.

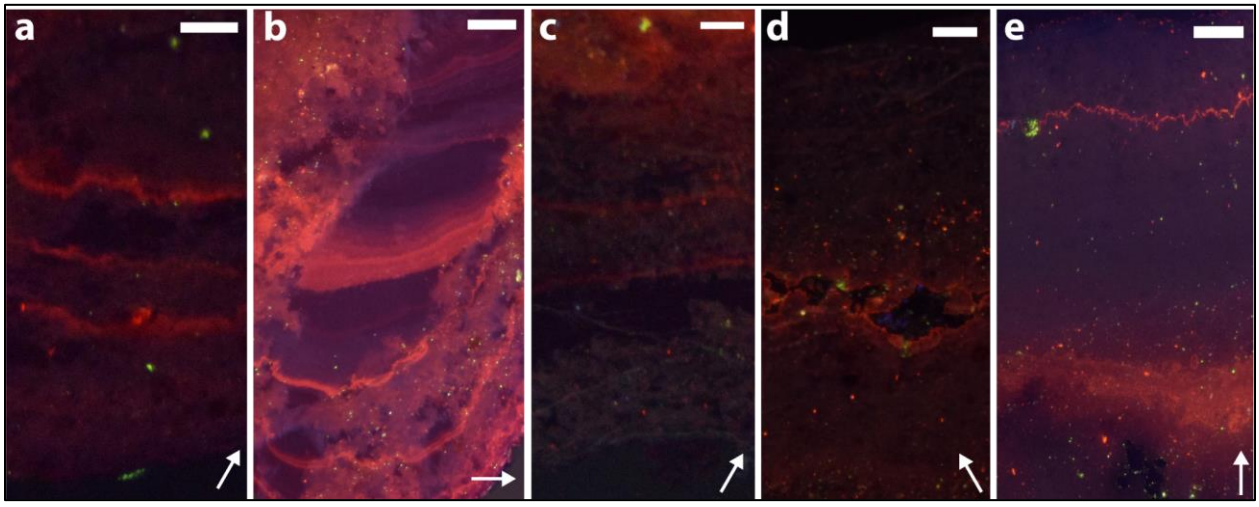

Figure 7. CL images showing examples of characteristic patterns at 9.0 m (A), 9.3 m (B), 9.4 m (C), 9.6 m (D), and 9.7 m (E). Concentric bands are common at shallower depths, varying in width and brightness even within the same set of bands (A-C). Nearing the oxic-anoxic transition, bands become rare; diffuse CL and non-luminescence are the most common patterns observed (D-E). Images are oriented such that crystal growth proceeds towards the top edge; arrows indicate direction to the mat-water interface. Scale bars are 100 μm.

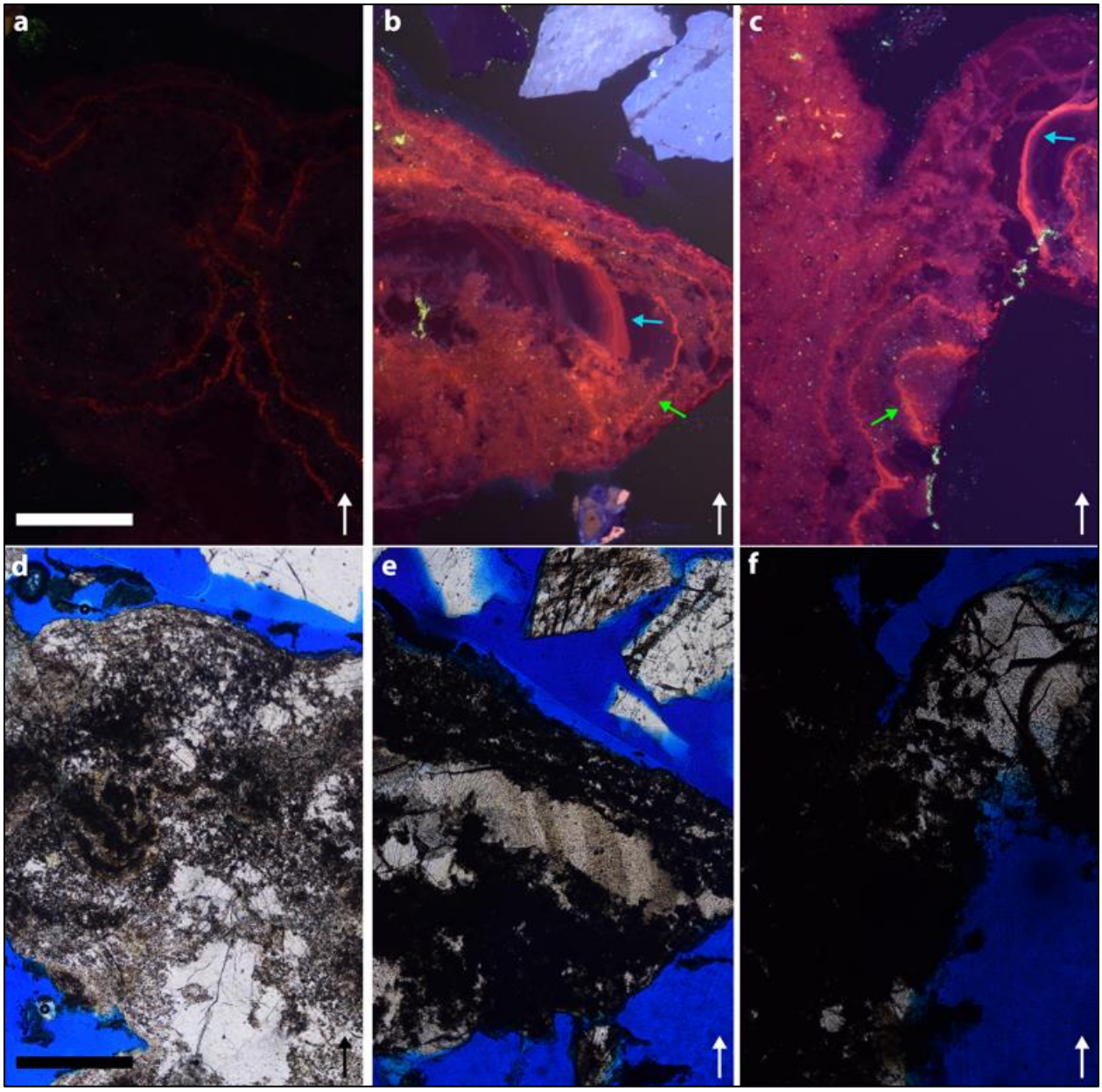

Figure 8. CL images (A-C) show concentric bands of red CL in carbonates from 9.0 m (A) and 9.3 m (B-C) separated by dim or non-luminescent zones. Bands in "clean" low-sediment carbonate (cyan arrows) are visually distinct with sharp edges, while bands in "dirty" high-sediment zones (green arrows) are less distinct and have wavy edges. Discoloration of carbonate visible in plane-polarized transmitted light (E-F) corresponds to bright CL bands (B-C) at 9.3 m. White/black arrows indicate direction to the mat-water interface. Scale bars are 500 μm.

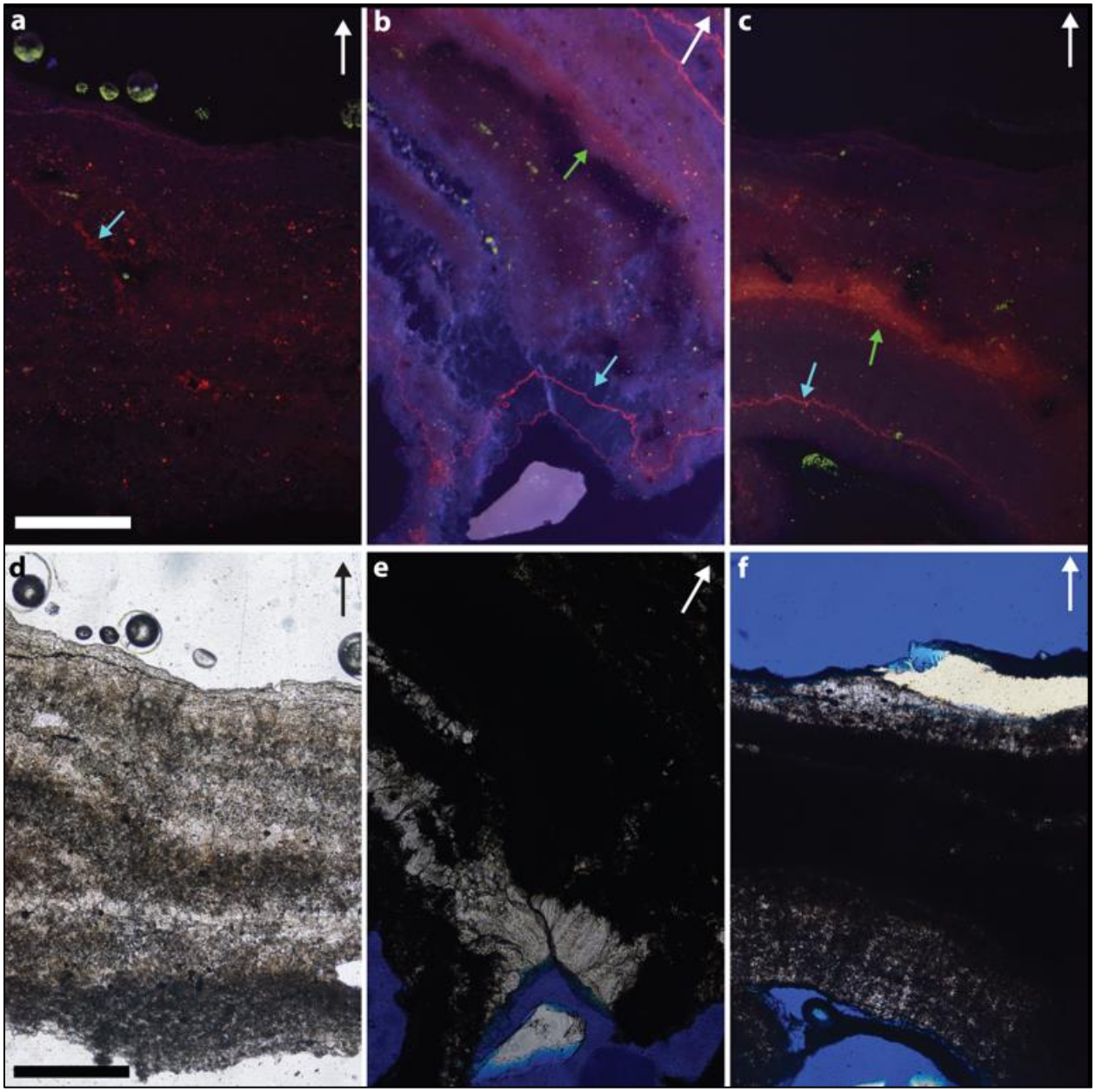

Figure 9. CL images (A-C) show that bright red luminescence is uncommon near the oxic-anoxic transition depth. Dim diffuse red to reddish-purple luminescence (B-C, green arrows) and very narrow bands (A-C, cyan arrows) are the most common CL patterns at these depths. Transmitted-light photographs (D-F) show that most carbonate at this depth has high sediment/organic matter content corresponding to very dim or non-luminescent CL zones. White/black arrows indicate direction to the mat-water interface. Scale bars are 500 μm.

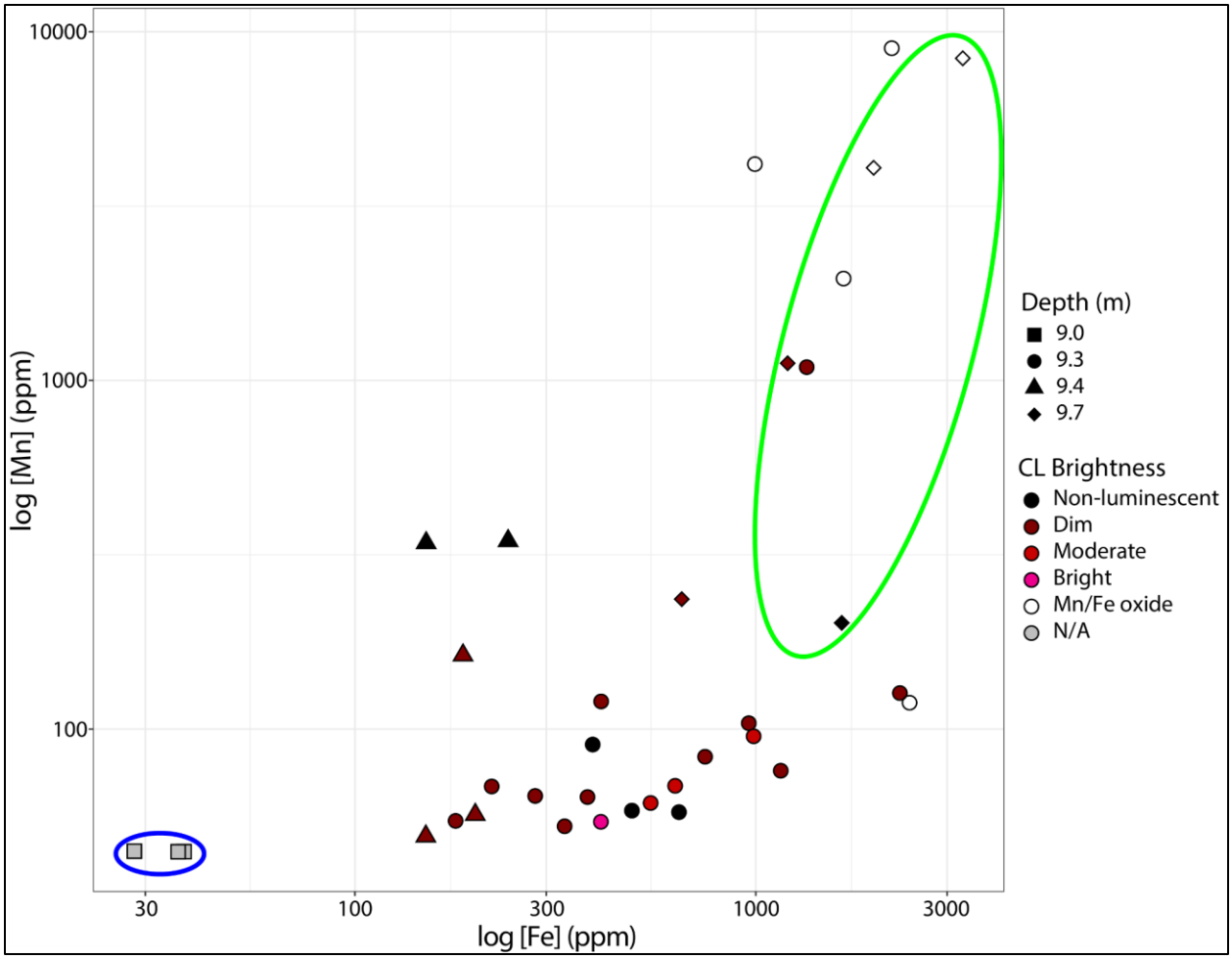

Figure 10. Log-log plot of Mn and Fe content of Lake Fryxell carbonates. Most carbonates (filled symbols) display low Mn content, with the majority of high Mn concentrations representative of Fe/Mn oxides (open symbols) entombed in carbonate. Dim CL is the most common across the range of Mn/Fe concentrations and ratios. The shallowest carbonates display the lowest concentrations of Mn and Fe (blue ellipse), and the deepest carbonates contain the most Mn and Fe (green ellipse).

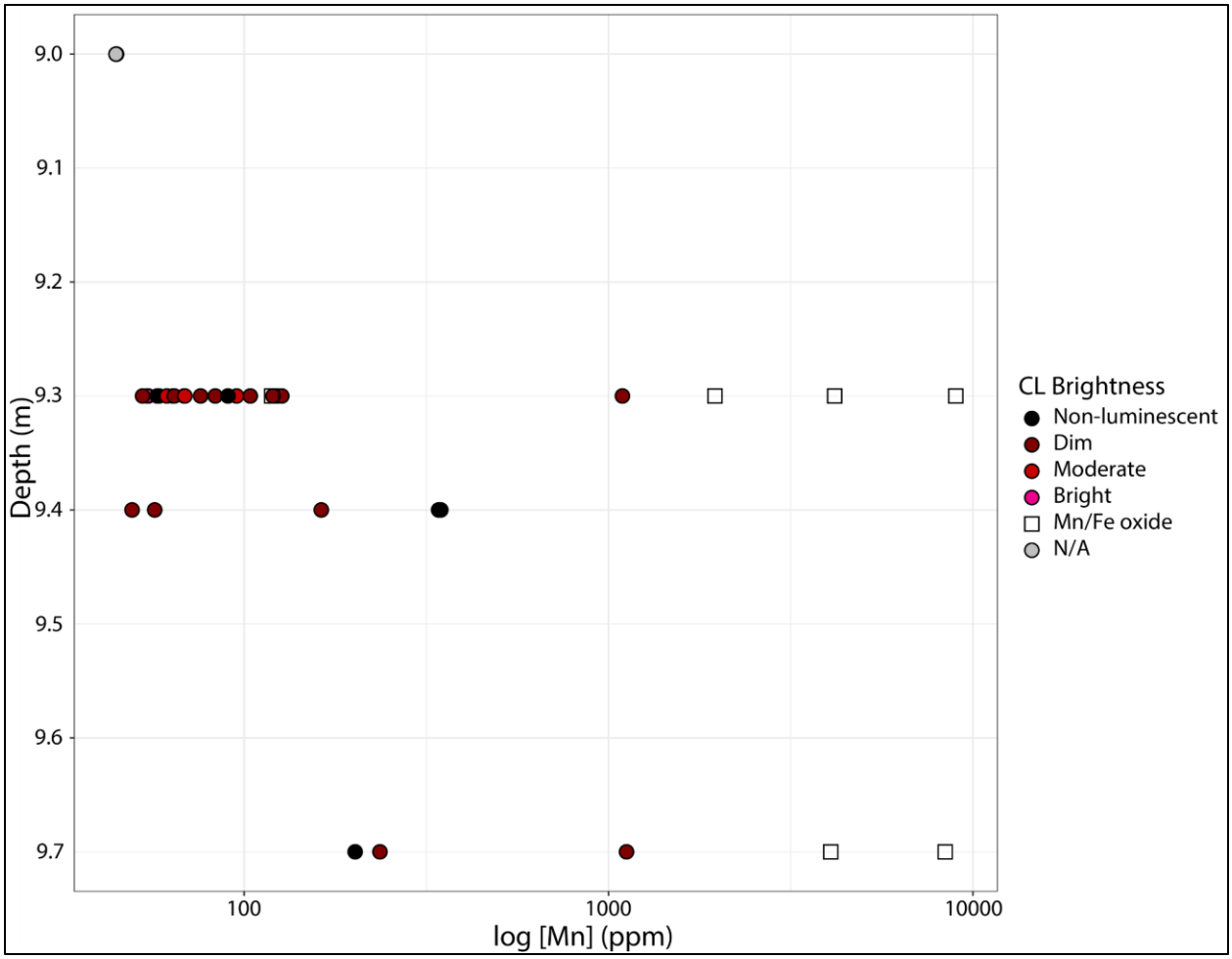

Figure 11. Minimum Mn concentration increases with depth. Mn concentration does not correlate with CL brightness, and shows the largest variance at 9.3 and 9.7 m. Mn concentrations of ~2000 ppm and above represent brown to black-colored spots, most likely insoluble Mn-Fe oxides entombed in carbonate.

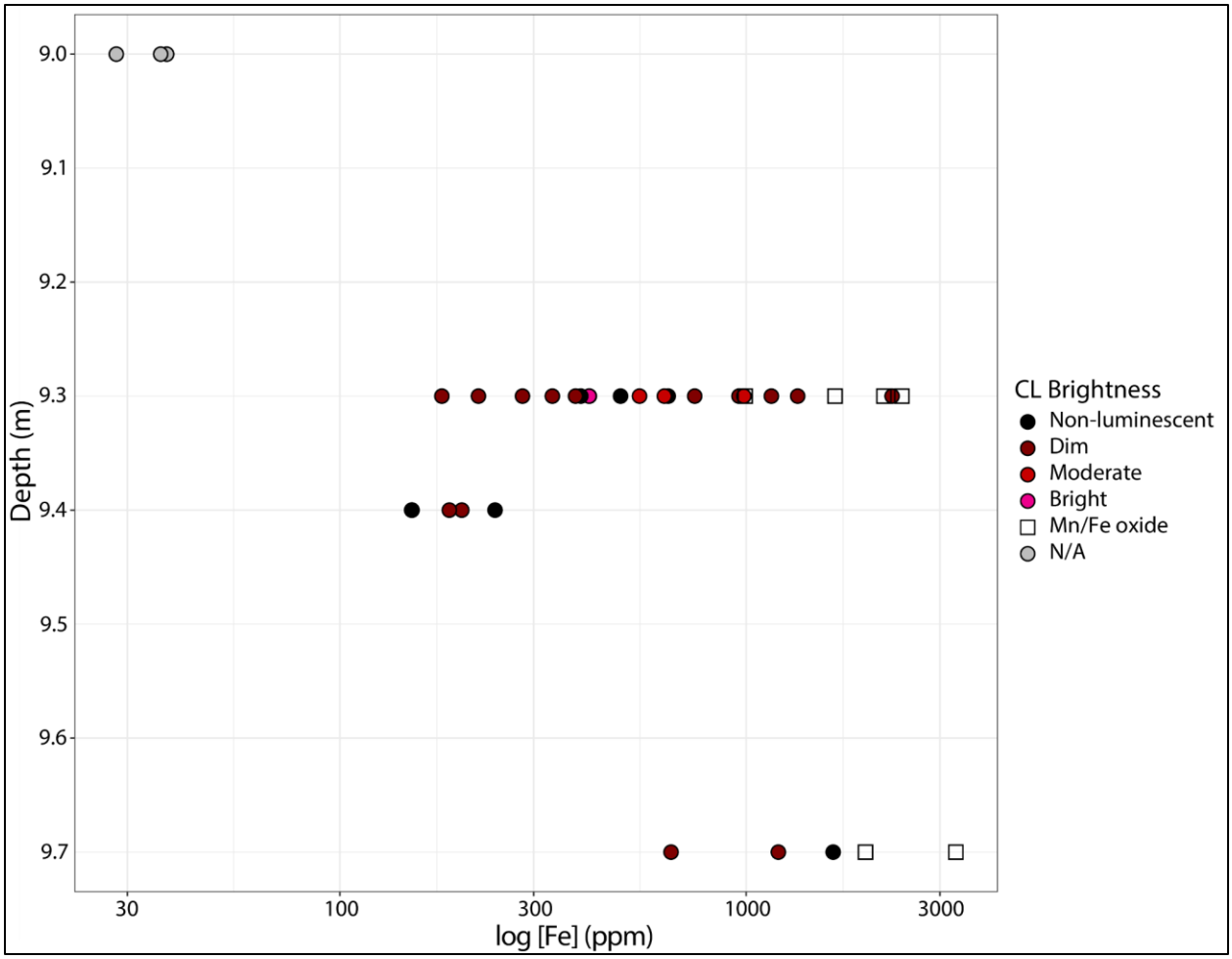

Figure 12. Minimum Fe concentration in carbonates increases with depth. Fe concentration does not correlate with CL brightness, and shows the largest variance at 9.3 m. Most Fe concentrations of ~1650 ppm and above represent brown to black-colored spots, most likely insoluble Mn-Fe oxides entombed in carbonate.

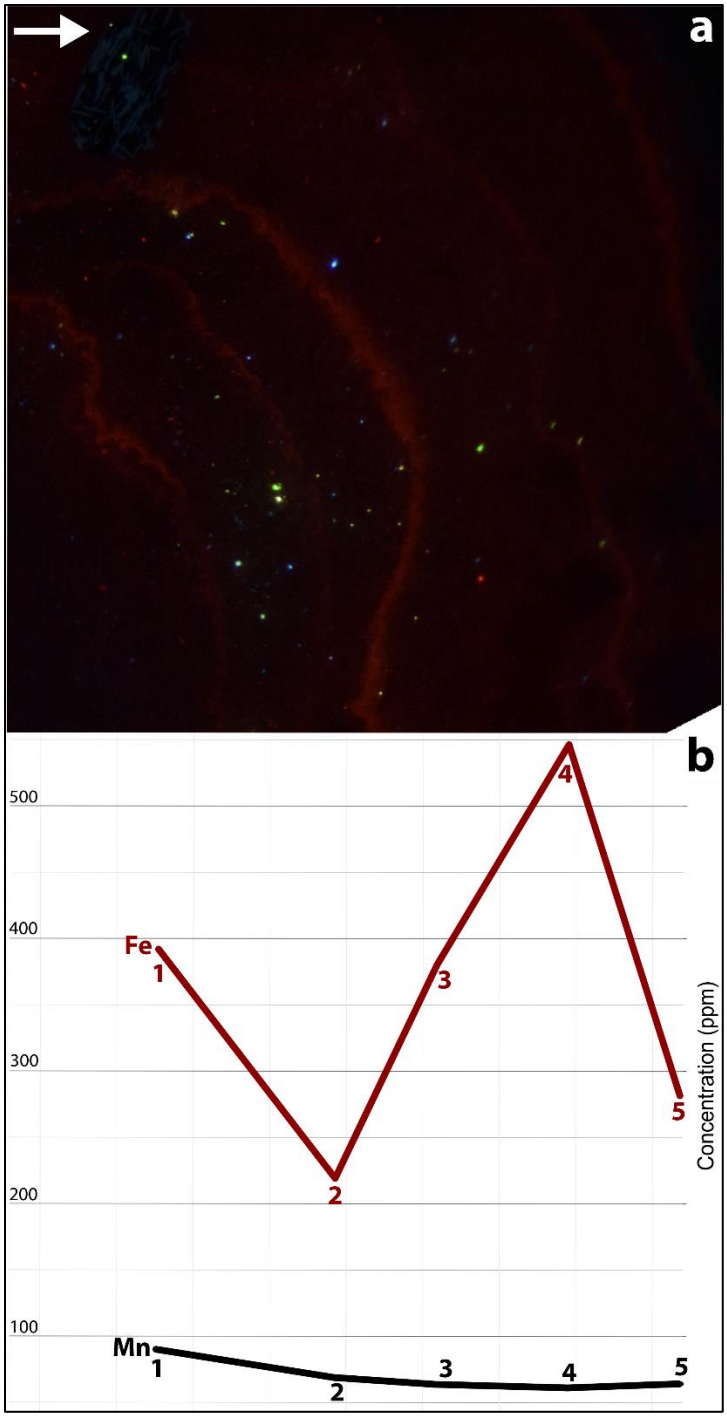

Figure 13. (A) CL bands at 9.3 m are concentric and convex in the direction of carbonate growth (white arrow). (B) Mn and Fe concentrations vary in the direction of carbonate growth, Mn over tens of ppm and Fe over hundreds of ppm. Numbers indicate LA-ICP-OES scan locations. The Fe/Mn ratio ranges from 3.20 (location 2) to 8.90 (location 4). Note the low Fe/Mn ratio (3.20) at location 2 corresponding to the brightest CL band in this area, and the slightly higher Fe/Mn ratio (4.38) at location 5 corresponding to a moderate-brightness band. The highest Fe/Mn ratio (8.90) in this area is at location 4, corresponding to a zone of very dim luminescence. White arrow indicates direction to the mat-water interface.

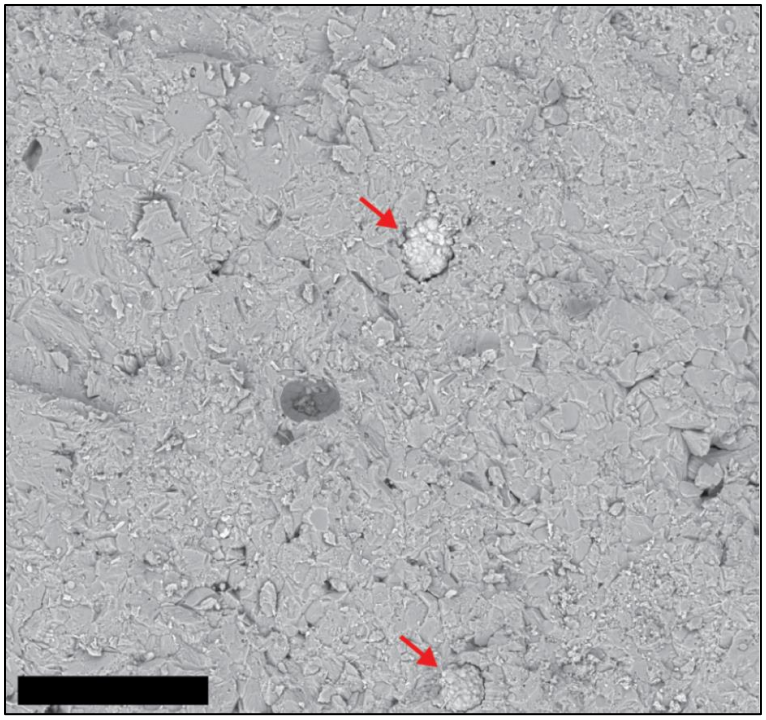

Figure 14. Scanning electron micrograph showing Mn-oxide spheroids (red arrows) entombed in calcite at the oxic-anoxic transition depth (9.7 m). Elemental composition confirmed by SEM-EDS (Figure S2). Scale bar is 100 μm.

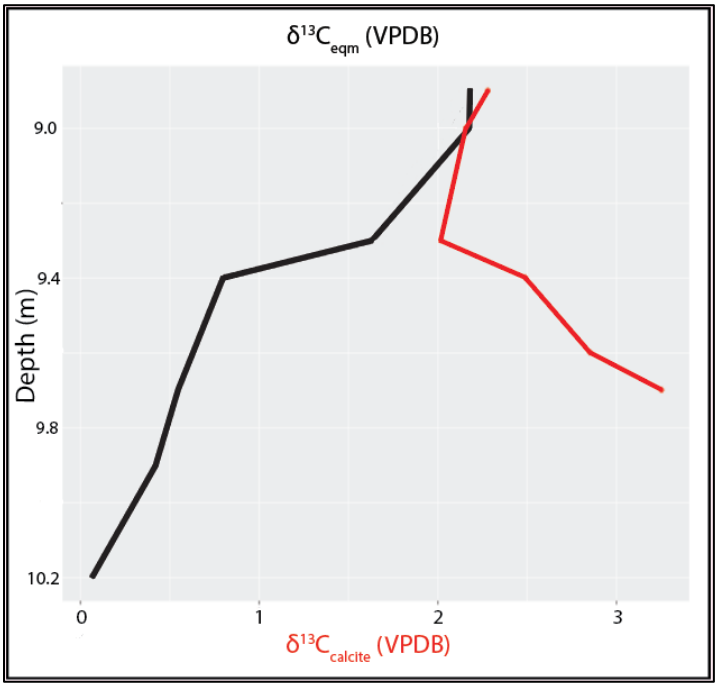

Figure 15. Average $\delta^{13}C$ of carbonates (red line) in the lower oxycline compared to expected values calculated for precipitation in isotopic equilibrium with water column DIC (black line) (after Romanek et al. 1992). Carbonates become more enriched in ^{13}C with depth in contrast to depletion of $\delta^{13}C_{DIC}$.

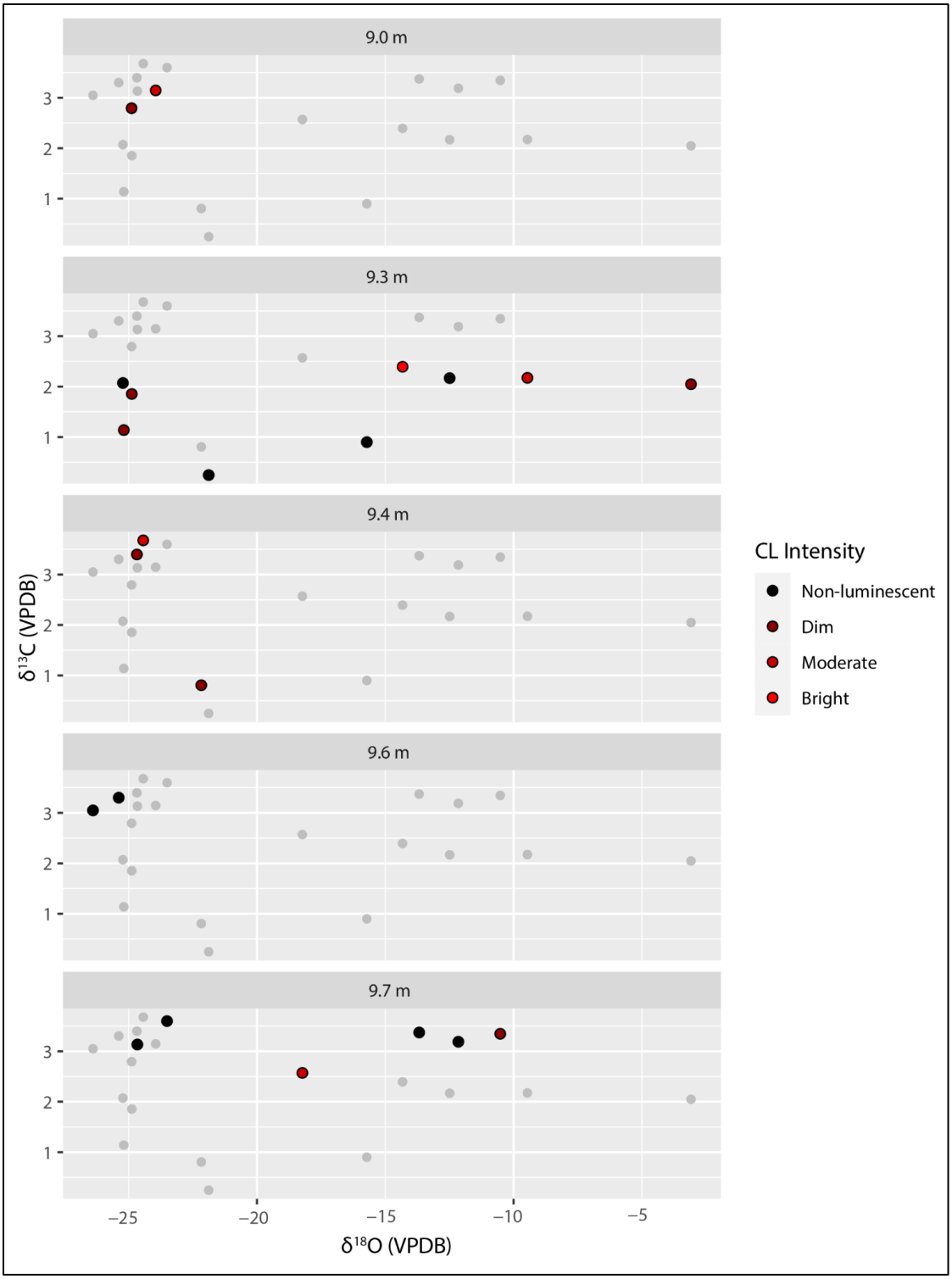

Figure 16. Lake Fryxell carbonates predominantly show slight enrichment (~1-3.25‰ VPDB) in ^{13}C throughout the lower oxycline due to removal of ^{12}C from the DIC pool by microbial metabolism. $\delta^{18}O$ varies widely in these samples, particularly at 9.3 m. $\delta^{13}C$ and $\delta^{18}O$ do not co-vary, and neither correlates with redox at the time of precipitation, as inferred from CL intensity.

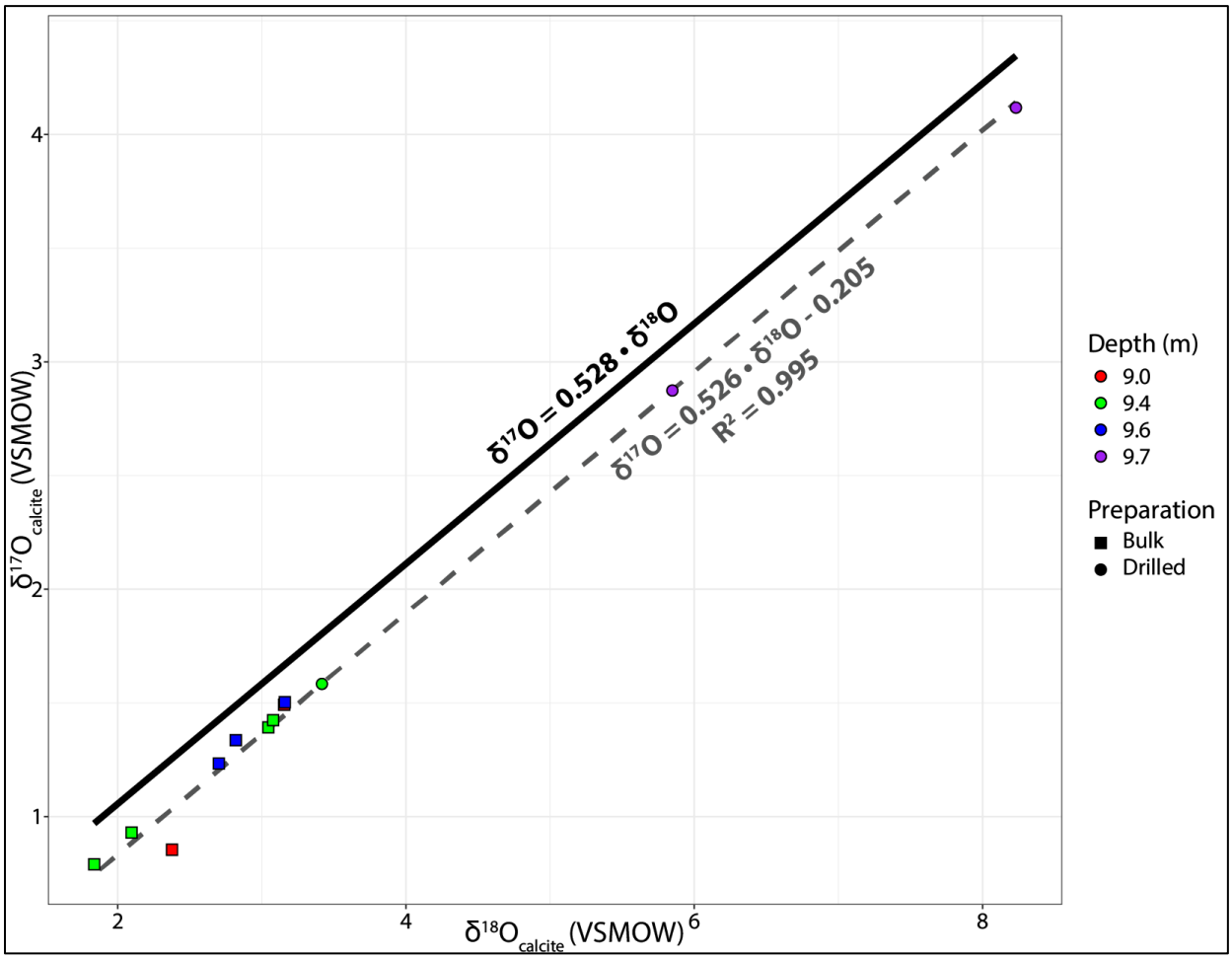

Figure 17. $\delta^{18}O_{calcite}$ vs. $\delta^{17}O_{calcite}$ yields a slope of 0.526, indicating mass-dependent fractionation of oxygen isotopes in Lake Fryxell. Drilled samples (circles) are enriched in both ^{18}O and ^{17}O relative to bulk samples (squares), indicating μm- to mm-scale variability in carbonate oxygen isotope composition which is not detectable in bulk samples due to homogenization of the carbonate during bulk sample preparation. Oxygen isotope variability shown here is in alignment with ^{18}O variability observed in traditional ^{13}C and ^{18}O analysis (see section IV, subsection vii, Figure 16). Neither $\delta^{18}O$ nor $\delta^{17}O$ covaries with water depth. Heavy black line represents the $\delta^{17}O$ values expected from the measured $\delta^{18}O$ values, as calculated by Equation (1).

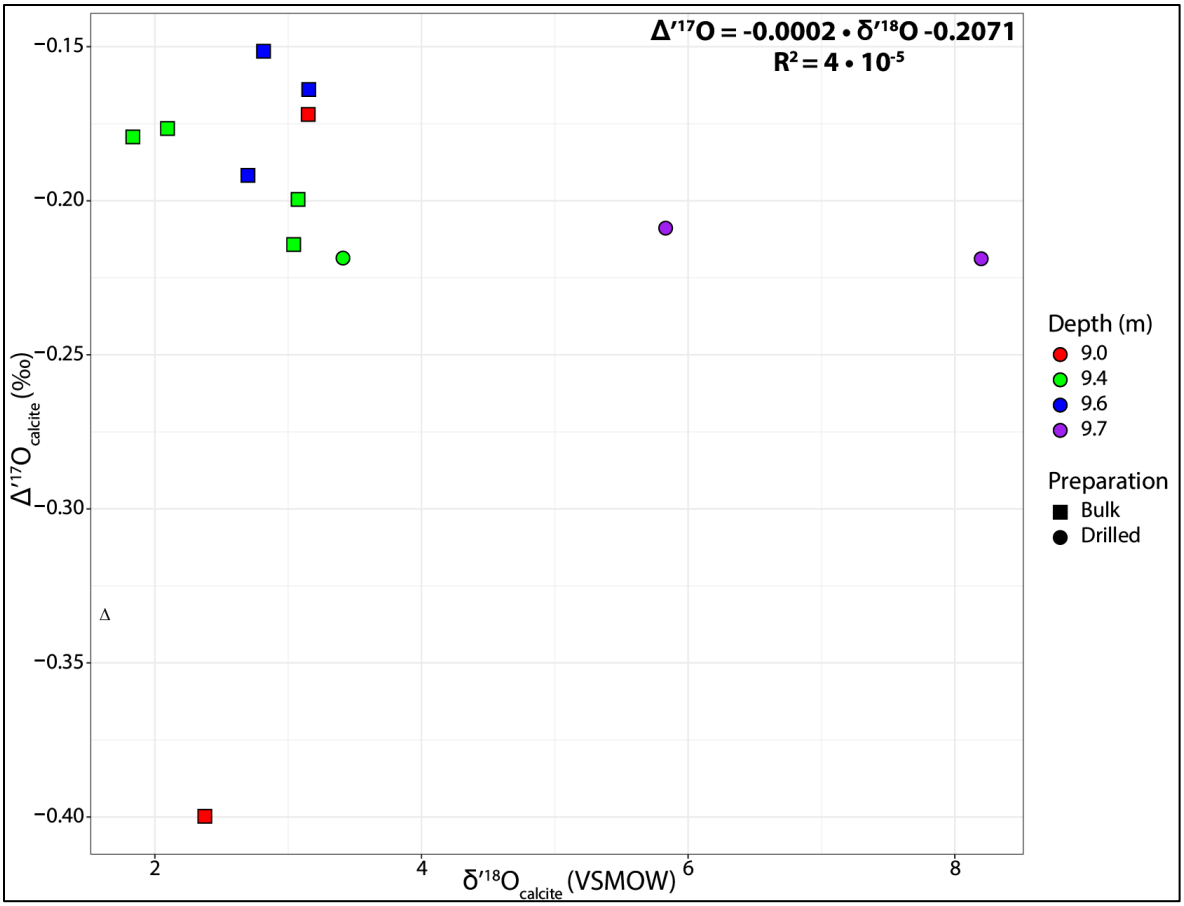

Figure 18. $\Delta'^{17}O$ is negative (-0.151 to -0.399‰) in all samples and does not covary with $\delta'^{18}O$ ($R^2 \approx 0$) or $\delta'^{17}O$ (not shown, $R^2 = 0.004$). $\Delta'^{17}O$ of drilled samples (circles) is not significantly different from that of bulk samples (squares). $\Delta'^{17}O/\delta'^{18}O$ plots significantly below equilibrium curves for precipitation of calcite from modern seawater (see Wostbrock and Sharp 2021), suggesting influence by a modified marine water on carbonate oxygen isotope composition.

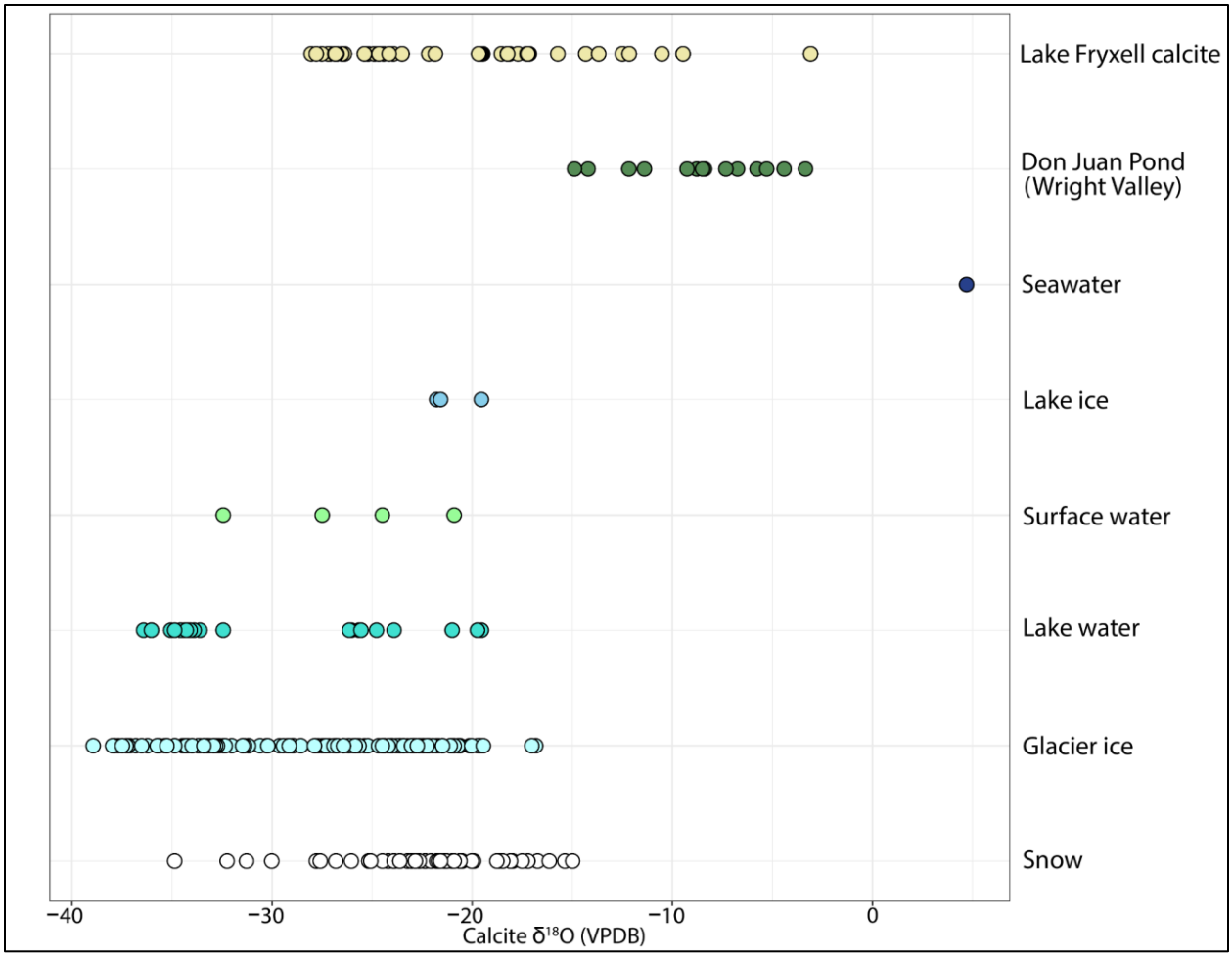

Figure 19. $\delta^{18}O$ values of Lake Fryxell calcite and predicted $\delta^{18}O$ values of calcite precipitated in isotopic equilibrium with different water sources. All waters except Don Juan Pond and seawater are sampled from Taylor Valley; seawater is assumed to have $\delta^{18}O$ = -29.99‰ VPDB (0‰ VSMOW). Seawater is the only available water whose $\delta^{18}O$ is high enough to fully explain the highest carbonate $\delta^{18}O$ values observed in Lake Fryxell calcite, suggesting mixing of marine-sourced waters with pore waters in the benthos of Lake Fryxell. Water $\delta^{18}O$ values from Matsubaya et al. (1979) and Fountain (2014). Calcite $\delta^{18}O$ predictions calculated following calcite-water fractionation factors in Wostbrock et al. (2020).

List of Appendices

Appendix A: Supplementary Data & Figures.....60

Appendix A: Supplementary Data & Figures

Table S1. Measured $\delta^{13}C$ and $\delta^{18}O$ values of Lake Fryxell carbonates (not including $\delta^{18}O$ from triple oxygen analysis). Each analytical run consisted of 12 measurements; values presented here are averages of these measurements. All data are permille values on the VPDB scale.

Sample	Depth (m)	$\delta^{13}C$	$\delta^{18}O$	Preparation
8.9 2012 #1	8.9	2.28	-19.47	Bulk
8.9 2012 #2	8.9	2.32	-19.56	Bulk
8.9 2012 #3	8.9	2.28	-19.64	Bulk
8.9 2012 #4	8.9	2.27	-19.52	Bulk
8.9 2012 #5	8.9	2.25	-19.57	Bulk
Dredge1 A #1	9.0	3.14	-23.94	Drilled
Dredge1 A #3	9.0	2.79	-24.88	Drilled
Dredge1 B #2	9.0	-1.09	-18.54	Drilled
9.3 2012 #1	9.3	2.43	-19.61	Bulk
9.3 2012 #2	9.3	2.43	-19.66	Bulk
9.3 2012 #3	9.3	2.41	-19.64	Bulk
9.3 2012 #4	9.3	2.42	-19.66	Bulk
9.3 2012 #5	9.3	2.43	-19.62	Bulk
9.3 2012 #6	9.3	2.42	-19.68	Bulk
LF 9.3 #2	9.3	2.39	-14.32	Drilled
LF 9.3 #3	9.3	2.17	-9.46	Drilled
LF 9.3 #4	9.3	2.04	-3.08	Drilled
LF 9.3 #5	9.3	2.16	-12.49	Drilled
LF 9.3#9	9.3	2.07	-25.22	Drilled
LF 9.3#10	9.3	0.89	-15.71	Drilled
LF 9.3#8	9.3	1.85	-24.87	Drilled

Table S1 (continued).

LF 9.3 #6	9.3	0.24	-21.88	Drilled
N-A.1	9.4	1.88	-18.19	Bulk
N-B.1	9.4	2.79	-17.20	Bulk
N-A.2 #1	9.4	3.67	-24.43	Drilled
N-A.2 #2	9.4	3.39	-24.67	Drilled
N-A.2 #4	9.4	0.80	-22.17	Drilled
N-A.2 #3	9.4	3.72	-17.71	Drilled
J.2-A	9.6	2.74	-17.22	Bulk
J.2-A #1	9.6	3.30	-25.38	Drilled
J.2-A #2	9.6	3.04	-26.39	Drilled
LF 9.7#6	9.7	1.13	-25.18	Drilled
16Nov12 #1	9.7	3.13	-24.66	Drilled
16Nov12 #2	9.7	3.59	-23.50	Drilled
LF 9.7 #2	9.7	3.18	-12.15	Drilled
LF 9.7 #3	9.7	3.37	-13.67	Drilled
LF 9.7#4	9.7	2.57	-18.23	Drilled
LF 9.7#5	9.7	3.34	-10.52	Drilled

Table S2. Mn and Fe concentrations in Lake Fryxell carbonates measured via LA-ICP-OES and CL brightness at each sampling site (1 = non-luminescent, 2 = dim, 3 = moderate, 4 = bright, 5 = Mn/Fe oxide, N/A = CL data not available). Concentrations in ppm.

Sample ID	Mn	Fe	Fe/Mn Ratio	Depth (m)	CL Brightness
Dredge1_B_blkspot	44.514	37.475	0.842	9.0	N/A
Dredge1_B_cleancarbonate	44.671	28.168	0.631	9.0	N/A
Dredge1_B_topendline	44.507	36.218	0.814	9.0	N/A

Table S2 (continued).

LF_9.3_DSC_0046	54.546	178.258	3.268	9.3	2
LF_9.3_DSC_0058	103.976	960.323	9.236	9.3	2
LF_9.3_DSC_0058_2read	83.325	747.080	8.966	9.3	2
LF_9.3_DSC_0075_1	126.859	2287.315	18.030	9.3	2
LF_9.3_DSC_0075_2	95.380	987.377	10.352	9.3	3
LF_9.3_lower_DSC_0139insd	120.044	411.235	3.426	9.3	2
LF_9.3_lower_DSC_0139out	54.212	410.619	7.574	9.3	4
LF_9.3_lower_DSC_0141_1	75.968	1153.820	15.188	9.3	2
LF_9.3_lower_DSC_0141_2	58.370	490.733	8.407	9.3	1
LF_9.3_lower_DSC_0145	57.789	643.005	11.127	9.3	1
LF_9.3_lower_DSC_0153spot	4173.247	994.626	0.238	9.3	5
LF_9.3_upper_blackspot	119.030	2418.053	20.315	9.3	5
LF_9.3_upper_brownspot	1959.555	1654.913	0.845	9.3	5
LF_9.3_upper_DSC_0040_1	90.300	391.789	4.339	9.3	1
LF_9.3_upper_DSC_0040_2	68.478	219.310	3.203	9.3	2
LF_9.3_upper_DSC_0040_3	63.851	380.220	5.955	9.3	2
LF_9.3_upper_DSC_0040_4	61.391	546.459	8.901	9.3	3
LF_9.3_upper_DSC_0040_5	64.310	281.537	4.378	9.3	2
LF_9.3_upper_DSC_0081_1	68.758	629.043	9.149	9.3	3
LF_9.3_upper_DSC_0081_2	52.647	333.419	6.333	9.3	2
LF_9.3_upper_DSC_0100edge	8972.555	2182.958	0.243	9.3	5
LF_9.3_upper_DSC_0100insd	1091.816	1339.266	1.227	9.3	2
N-A.2_darkpatch_middle	346.558	240.963	0.695	9.4	1
N-A.2_inner	56.836	199.551	3.511	9.4	2

Table S2 (continued).

N-A.2_outeredge_cleancarb	49.265	150.217	3.049	9.4	2
N-A.2_outeredge_darkbump2	341.794	150.514	0.440	9.4	1
N-A.2_upperdarkarea	162.867	185.992	1.142	9.4	2
16Nov12_blkspot1	8393.344	3282.849	0.391	9.7	5
16Nov12_blkspot2_topleft	4071.994	1967.111	0.483	9.7	5
16Nov12_calcite	235.897	653.432	2.770	9.7	2
16Nov12_calcitetopedge	201.677	1637.671	8.120	9.7	1
16Nov12_calciteupper	1120.370	1200.256	1.071	9.7	2

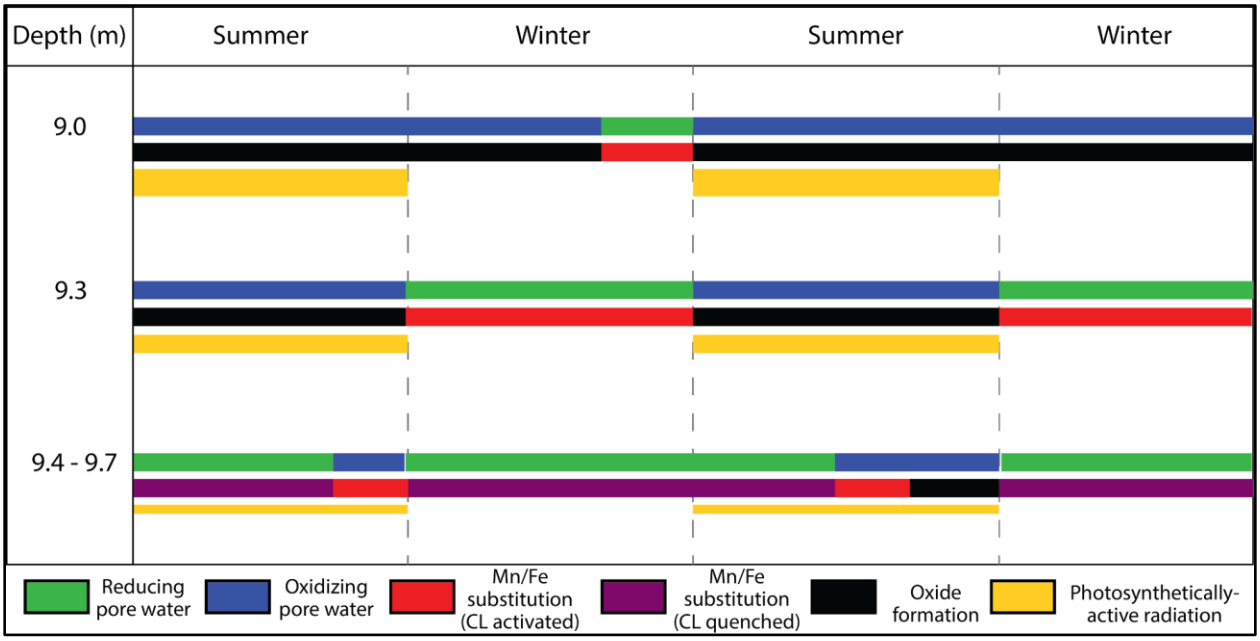

Figure S1. Paragenetic sequence diagram summarizing the changes in redox and Mn/Fe behavior in Lake Fryxell pore waters through time, as inferred from CL images and LA-ICP-OES data. Width of yellow lines represents the relative amount of PAR at each depth. Time is represented arbitrarily.

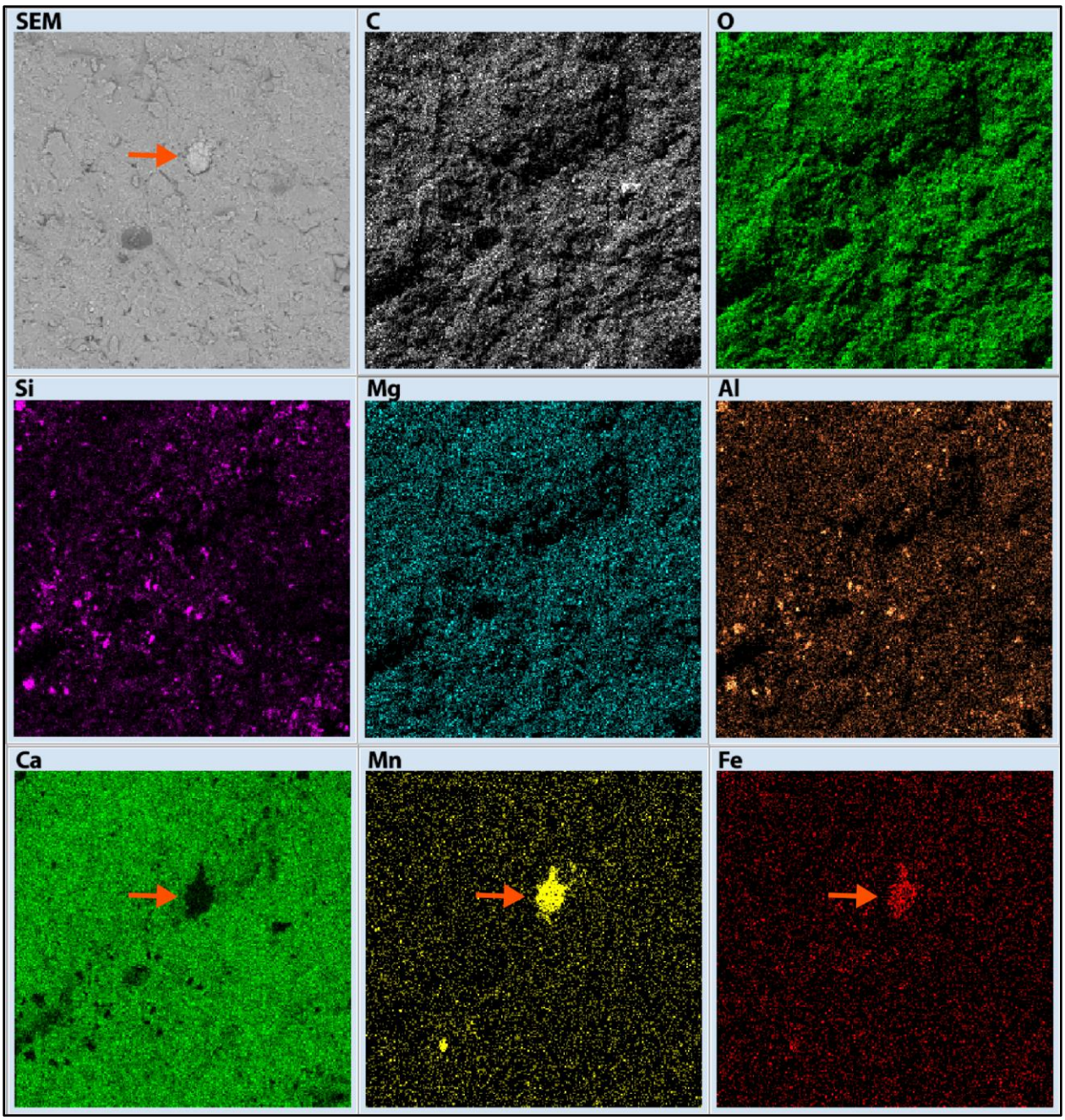

Figure S2. SEM-EDS maps of carbonate from 9.7 m depth. Brighter zones represent higher concentrations of the respective element. Zones of high Mn and Fe coincide with each other and with a zone of low Ca (orange arrows, bottom row), indicating that the small spheroid body visible in the SEM image (orange arrow, top left) is a Mn- and Fe-bearing oxide entombed in the calcite. The spheroid body is approximately 30 μm in diameter.

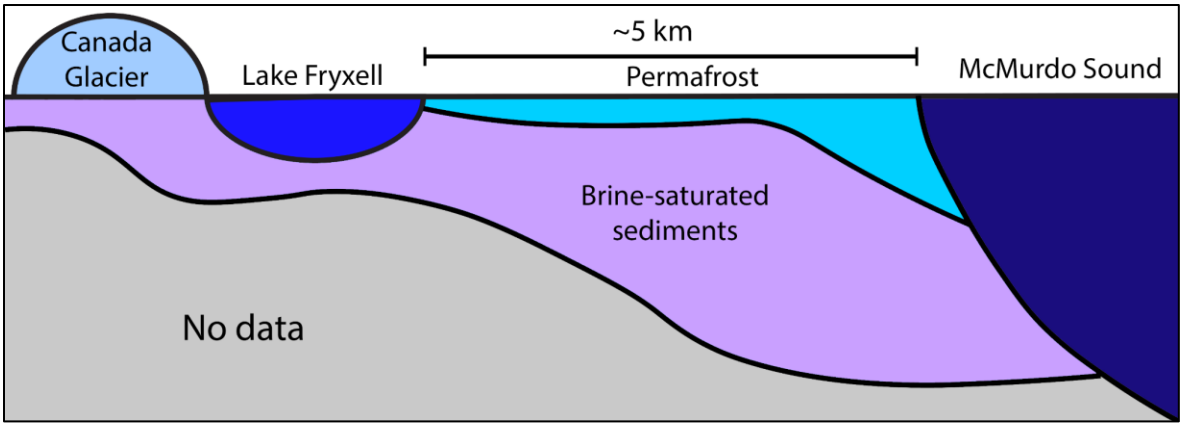

Figure S3. A calcium chloride-rich brine is present in the subsurface of Taylor Valley, connecting to Lake Fryxell and to the ocean at the McMurdo Sound. The extent of the brine has been mapped by aerial electromagnetic surveys. Figure not to scale. (Adapted from Mikucki et al. 2015).

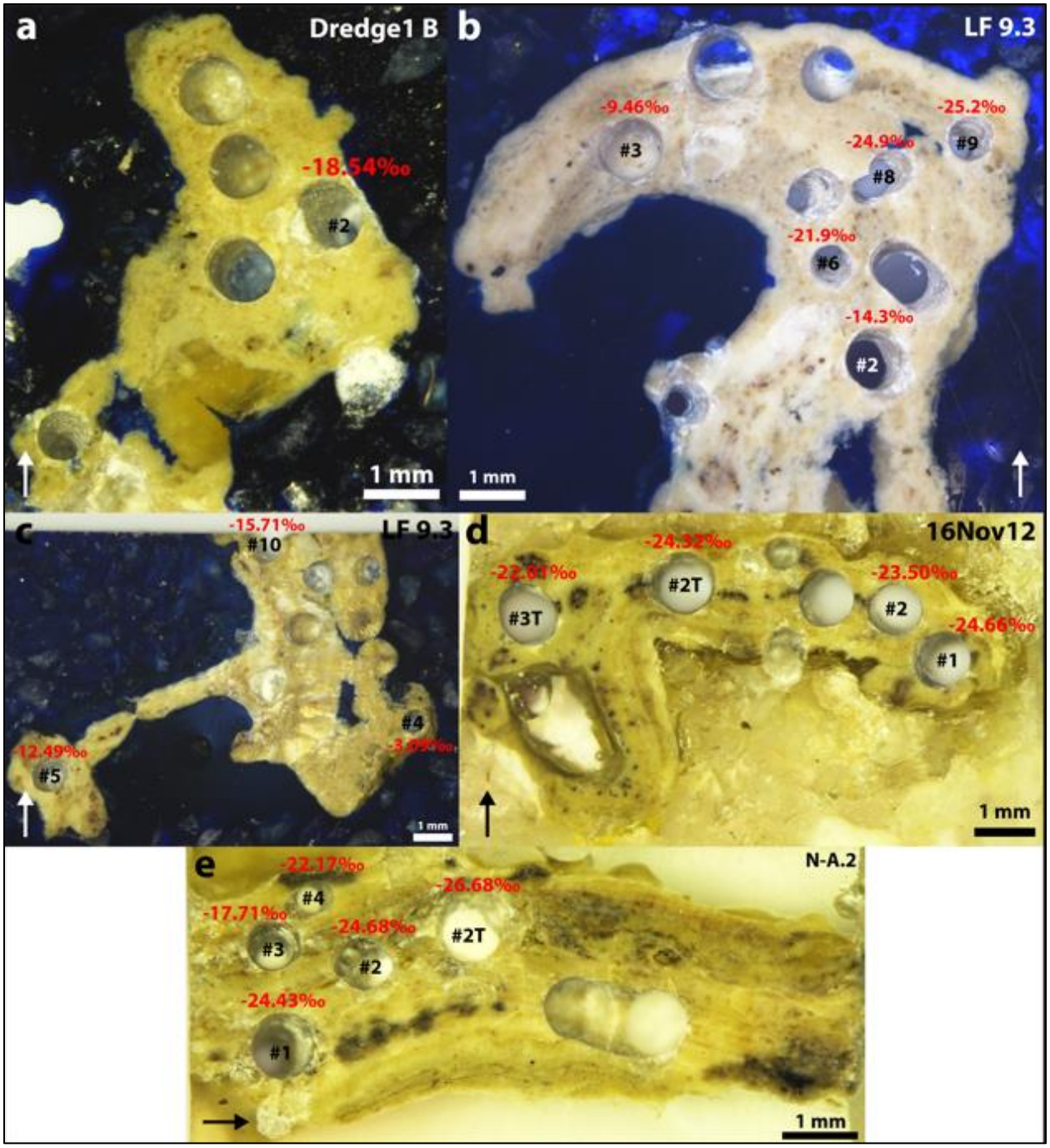

Figure S4. Reflected-light photomicrographs of selected subsampling sites for stable isotope analysis. Carbonate $\delta^{18}O$ is highly variable at sites separated by microns to millimeters, covering a range of approximately 24‰ in samples from 9.0 m (A), 9.3 m (B-C), 9.7 m (D), and 9.4 m (E). $\delta^{18}O$ values correspond to the labeled drill sites; site labels ending in T indicate sites sampled for triple oxygen isotope analysis. White/back arrows indicate direction to the mat-water interface. Values are presented relative to the VPDB standard.

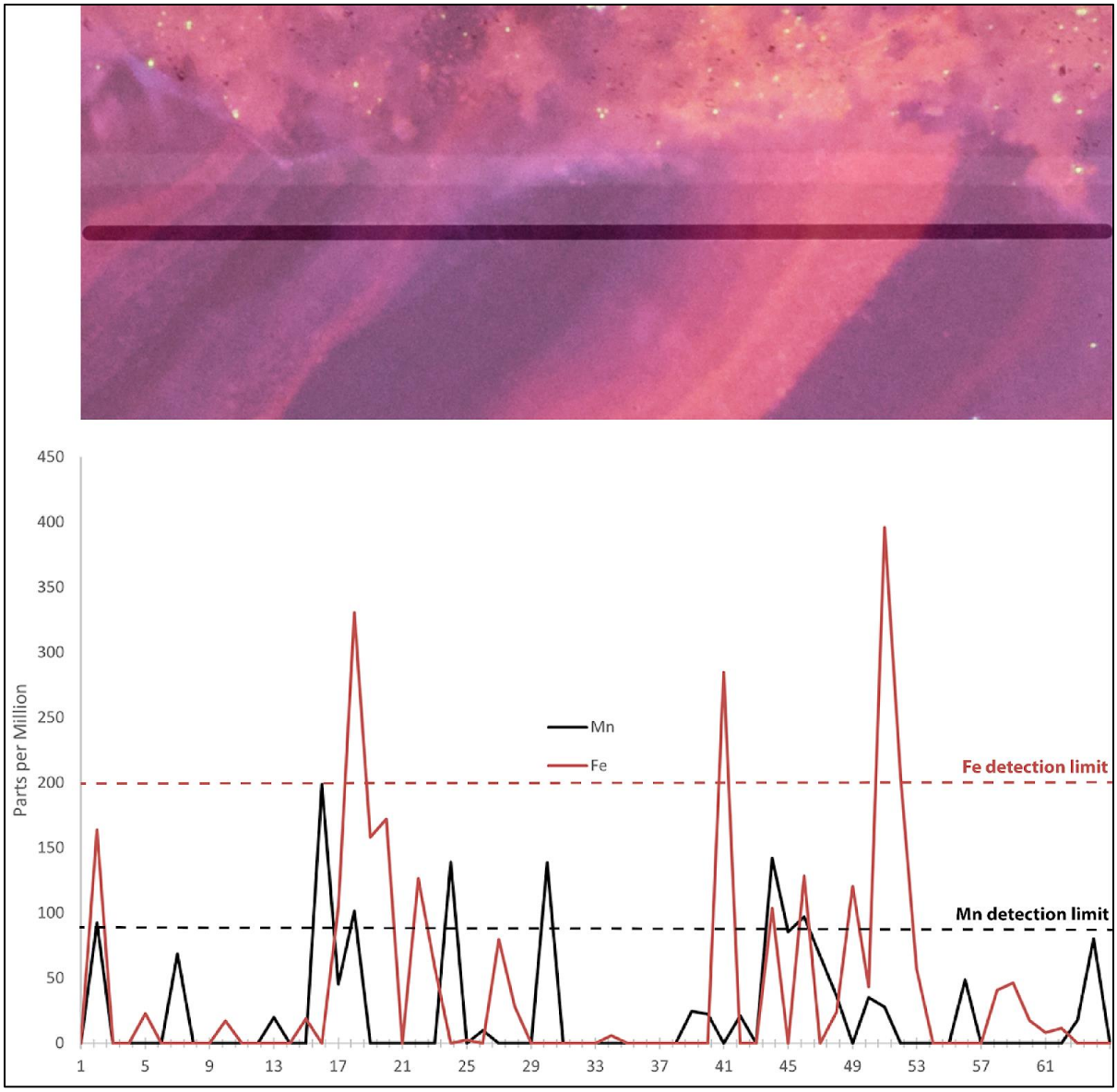

Figure S5. Electron microprobe transect across CL bands in carbonate from 9.3 m (see Figure 8B) shows variability in Fe/Mn ratio approximately corresponding to CL brightness. Shaded horizontal line represents the scanning path. Detection limits are 95±5 ppm for Mn and 210±9 ppm for Fe.

References

Braithwaite, C. (2016) Cathodoluminescence in Quaternary carbonate deposits. *Sedimentary Geology*, **337**, 29-35.

Cathey, D., Parker, B., Simmons Jr., G., Yongue Jr., W., and Van Brunt, M. (1981) The microfauna of algal mats and artificial substrates in Southern Victoria Land lakes of Antarctica. *Hydrobiologia*, **85**, 3-15.

Christ, A., and Bierman, P. (2020) The local Last Glacial Maximum in McMurdo Sound, Antarctica: Implications for ice-sheet behavior in the Ross Sea Embayment. *Geological Society of America Bulletin*, **132**, 31-47.

Clayton-Greene, J., Hendy, C., and Hogg, A. (1988) Chronology of a Wisconsin age proglacial lake in the Miers Valley, Antarctica. *New Zealand Journal of Geology and Geophysics*, **31**, 353-361.

Craig, H., Wharton, R., and McKay, C. (1992) Oxygen Supersaturation in Ice-Covered Antarctic Lakes: Biological Versus Physical Contributions. *Science*, **255**, 318-321.

Coplen, T. (2007) Calibration of the calcite-water oxygen-isotope geothermometer at Devils Hole, Nevada, a natural laboratory. *Geochimica et Cosmochimica Acta*, **71**, 3948-3957.

Davison, W. (1993) Iron and manganese in lakes. *Earth-Science Reviews*, **34**, 119-163.

Dietzel, M., Tang, J., Leis, A., and Köhler, S. (2009) Oxygen isotopic fractionation during inorganic calcite precipitation – Effects of temperature, precipitation rate and pH. *Chemical Geology*, **268**, 107-115.

Dillon, M., Hawes, I., Jungblut, A., Mackey, T., Eisen, J., Doran, P., and Sumner, D. (2020a) Energetic and Environmental Constraints on the Community Structure of Benthic Microbial Mats in Lake Fryxell, Antarctica. *FEMS Microbiology Ecology*, **96**, 1-10.

Dillon, M., Hawes, I., Jungblut, A., Mackey, T., Eisen, J., Doran, P., and Sumner, D. (2020b) Environmental control on the distribution of metabolic strategies of benthic microbial mats in Lake Fryxell, Antarctica. *PLoS ONE*, **15**.

Doran, P., and Gooseff, M. (2020) Lake level surveys in the McMurdo Dry Valleys, Antarctica (1991-2020, ongoing). *Environmental Data Initiative.*

Dowling, C., Lyons, W. (2014) Gas, Tritium, Stable Isotope, and Major Ion data for lake waters: 2005-2006 Antarctic Season. *McMurdo Dry Valleys LTER.*

Dromgoole, E., and Walter, L. (1990) Iron and manganese incorporation into calcite: Effects of growth kinetics, temperature and solution chemistry. *Chemical Geology,* **81**, 311-336.

Dugan, H., Obryk, M., and Doran, P. (2013) Lake ice ablation rates from permanently ice-covered Antarctic lakes. *Journal of Glaciology,* **59**, 491-498.

Foley, N., Tulaczyk, S., Grombacher, D., Doran, P., Mikucki, J., Myers, K., Foged, N., Dugan, H., Auken, E., and Virginia, R. (2019) Evidence for Pathways of Concentrated Submarine Groundwater Discharge in East Antarctica from Helicopter-Borne Electrical Resistivity Measurements. *Hydrology,* **6**, 1-15.

Fountain, A. (2014) Isotope Ratios of Ice and Snow in Taylor Valley. *McMurdo Dry Valleys LTER.*

Gabitov, R., Watson, E., and Sadekov, A. (2012) Oxygen isotope fractionation between calcite and fluid as a function of growth rate and temperature: An in situ study. *Chemical Geology,* **306-307**, 92-102.

Gunasekaran, S., Anbalagan, G., and Pandi, S. (2006) Raman and infrared spectra of carbonates of calcite structure. *Journal of Raman Spectroscopy,* **37**, 892-899.

Hall, B., and Denton, G. (2000) Radiocarbon Chronology of Ross Sea Drift, Eastern Taylor Valley, Antarctica: Evidence for a Grounded Ice Sheet in the Ross Sea at the Last Glacial Maximum. *Geografiska Annaler,* **82**, 305-336.

Hall, B., Denton, G., and Hendy, C. (2000) Evidence from Taylor Valley for a grounded ice sheet in the Ross Sea, Antarctica. *Geografiska Annaler,* **82**, 275-303.

Hall, B., Denton, G., Heath, S., Jackson, M., and Koffman, T. (2015) Accumulation and marine forcing of ice dynamics in the western Ross Sea during the last deglaciation. *Nature Geoscience,* **8**, 625-629.

Harnish, R., Ranville, J., McKnight, D., and Spaulding, S. (1991) Redox-mediated cycling of iron and manganese in Lake Fryxell: Associations with particulate, colloidal, and dissolved forms. *Antarctic Journal of the United States,* **3**, 230-232.

Harris, K., Carey, A., Lyons, W., Welch, K., and Fountain, A. (2007) Solute and isotope geochemistry of subsurface ice melt seeps in Taylor Valley, Antarctica. *Geological Society of America Bulletin*, **119**, 548-555.

Hawes, I., Sumner, D., Andersen, D., and Mackey, T. (2011) Legacies of recent environmental change in the benthic communities of Lake Joyce, a perennially ice-covered Antarctic lake. *Geobiology,* **9**, 394-410.

Hiatt, E., and Pufahl, P. (2014) Chapter 5: Cathodoluminescence Petrography of Carbonate Rocks: A Review of Applications for Understanding Diagenesis, Reservoir Quality, and Pore System Evolution. *Mineralogical Association of Canada Short Course,* **45**, 75-96.

Horita, J. (2009) Isotopic Evolution of Saline Lakes in the Low-Latitude and Polar Regions. *Aquatic Geochemistry,* **15**, 43-69.

Jungblut, A., Hawes, I., Mackey, T., Krusor, M., Doran, P., Sumner, D., Eisen, J., Hillman, C., and Goroncy, A. (2016) Microbial Mat Communities along an Oxygen Gradient in a Perennially Ice-Covered Antarctic Lake. *Applied and Environmental Microbiology*, **82**, 620-630.

Karr, E., Sattley, W., Rice, M., Jung, D., Madigan, M., and Achenbach, L. (2005a) Diversity and Distribution of Sulfate-Reducing Bacteria in Permanently Frozen Lake Fryxell, McMurdo Dry Valleys, Antarctica. *Applied and Environmental Microbiology,* **71**, 6353-6359.

Karr, E., Ng, J., Belchik, S., Sattley, W., Madigan, M., and Achenbach, L. (2005b) Biodiversity of Methanogenic and Other *Archaea* in the Permanently Frozen Lake Fryxell, Antarctica. *Applied and Environmental Microbiology*, **72**, 1663-1666.

Kim, S., and O'Neil, J. (1997) Equilibrium and nonequilibrium oxygen isotope effects in synthetic carbonates. *Geochimica et Cosmochimica Acta*, **61**, 3461-3475.

Knoepfle, J., Doran, P., Kenig, F., Lyons, W., and Galchenko, V. (2009) Particulate organic and dissolved inorganic carbon isotopic compositions in Taylor Valley lakes, Antarctica: the effect of legacy. *Hydrobiologia*, **632**, 139-156.

Lawrence, M., and Hendy, C. (1985) Water column and sediment characteristics of Lake Fryxell, Taylor Valley, Antarctica. *New Zealand Journal of Geology and Geophysics*, **28**, 543-552.

Lawrence, M., and Hendy, C. (1989) Carbonate deposition and Ross Sea ice advance, Fryxell basin, Taylor Valley, Antarctica. *New Zealand Journal of Geology and Geophysics*, **32**, 267-278.

Laybourn-Parry, J., James, M., McKnight, D., Priscu, J., Spaulding, S., and Shiel, R. (1997) The microbial plankton of Lake Fryxell, southern Victoria Land, Antarctica during the summers of 1992 and 1994. *Polar Biology*, **17**, 54-61.

Lea, D., Martin, P., Pak, D., and Spero, H. (2002) Reconstructing a 350 ky history of sea level using planktonic Mg/Ca and oxygen isotope records from a Cocos Ridge core. *Quaternary Science Reviews*, **21**, 283-293.

Mackey, T., Sumner, D., Hawes, I., Jungblut, A., and Andersen, D. (2015) Growth of modern branched columnar stromatolites in Lake Joyce, Antarctica. *Geobiology*, **13**, 373-390.

Mackey, T., Sumner, D., Hawes, I., Andersen, D., and Jungblut, A. (2018) Stromatolite records of environmental change in perennially ice-covered Lake Joyce, McMurdo Dry Valleys, Antarctica. *Biogeochemistry*, **137**, 73-92.

Matsubaya, O., Sakai, H., Torii, T., Burton, H., and Kerry, K. (1979) Antarctic saline lakes – stable isotopic ratios, chemical compositions and evolution. *Geochimica et Cosmochimica Acta*, **43**, 7-25.

Mikucki, J., Auken, E., Tulaczyk, S., Virginia, R., Schamper, C., Sørensen, K., Doran, P., Dugan, H., and Foley, N. (2015) Deep groundwater and potential subsurface habitats beneath and Antarctic dry valley. *Nature Communications,* **6**, 1-9.

Miller, L., and Aiken, G. (1996) Effects of Glacial Meltwater Inflows and Moat Freezing on Mixing in an Ice-Covered Antarctic Lake as Interpreted from Stable Isotope and Tritium Distributions. *Limnology and Oceanography,* **41**, 966-976.

Myers, K., Doran, P., Tulaczyk, S., Foley, N., Bording, T., Auken, E., Dugan, H., Mikucki, J., Foged, N., Grombacher, D., and Virginia, R. (2021) Thermal legacy of a large paleolake in Taylor Valley, East Antarctica as evidenced by an airborne electromagnetic survey. *The Cryosphere,* **15**, 3577-3593.

Nealson, K. (2006) The Manganese-Oxidizing Bacteria. *Prokaryotes,* **5**, 222-231.

Neumann, K., Lyons, W., and Des Marais, D. (1998) Inorganic carbon-isotope distribution and budget in the Lake Hoare and Lake Fryxell basins, Taylor Valley, Antarctica. *Annals of Glaciology,* **27**, 685-690.

Neumann, K., Lyons, W., Priscu, J., Des Marais, D., and Welch, K. (2004) The carbon isotopic composition of dissolved inorganic carbon in perennially ice-covered Antarctic lakes: searching for a biogenic signature. *Annals of Glaciology,* **39**, 518-524.

Pesenti, H., Leoni, M., and Scardi, P. (2008) XRD line profile analysis of calcite powders produced by high energy milling. *Zeitschrift für Kristallographie Supplements,* **27**, 143-150.

Priscu, J. (2018) Dissolved Inorganic Carbon Concentrations in Lakes. *McMurdo Dry Valleys LTER.*

Priscu, J. (2018) Ice Thickness for Taylor Valley Lakes, Antarctica (1989-2018, ongoing). *McMurdo Dry Valleys LTER.*

Priscu, J. (2019) Hydrogen ion concentrations (pH) in discrete water column samples collected from lakes in the McMurdo Dry Valleys, Antarctica (1993-2018, ongoing). *McMurdo Dry Valleys LTER.*

Priscu, J. (2021) Underwater photosynthetically active radiation (PAR) vertical profiles collected from lakes in the McMurdo Dry Valleys, Antarctica (1993-2020, ongoing). *McMurdo Dry Valleys LTER.*

Rivera-Hernandez, F., Sumner, D., Mackey, T., Hawes, I., and Andersen, D. (2019) In a PICL: The sedimentary deposits and facies of perennially ice-covered lakes. *Sedimentology,* **66**, 917-939.

Roberts, E., Laybourn-Parry, J., McKnight, D., and Novarino, G. (2000) Stratification and dynamics of microbial loop communities in Lake Fryxell, Antarctica. *Freshwater Biology,* **44**, 649-661.

Romanek, C., Grossman, E., and Morse, J. (1992) Carbon isotopic fractionation in synthetic aragonite and calcite: Effects of temperature and precipitation rate. *Geochimica et Cosmoschimica Acta,* **56**, 419-430.

Sattley, W., and Madigan, M. (2006) Isolation, Characterization, and Ecology of Cold-Active, Chemolithotrophic, Sulfur-Oxidizing Bacteria from Perennially Ice-Covered Lake Fryxell, Antarctica. *Applied and Environmental Microbiology*, **72**, 5562-5568.

Sharp, Z., Wostbrock, J., and Pack, A. (2018) Mass-dependent triple oxygen isotope variations in terrestrial materials. *Geochemical Perspectives Letters*, **7**, 27-31.

Srivastava, R., Ramesh, R., Prakash, S., Anilkumar, N., and Sudhakar, M. (2007) Oxygen isotope and salinity variations in the Indian sector of the Southern Ocean. *Geophysical Research Letters,* **34**, 1-4.

Steig, E., Morse, D., Waddington, E., Stuiver, M., Grootes, P., Mayewski, P., Twickler, M., and Whitlow, S. (2000) Wisconsinan and Holocene climate history from an ice core at Taylor Dome, western Ross Embayment, Antarctica. *Geografiska Annaler,* **82**, 213-235.

Sumner, D., Hawes, I., Mackey, T., Jungblut, A., and Doran, P. (2015) Antarctic microbial mats: A modern analog for Archean lacustrine oxygen oases. *Geology,* **43**, 887-890.

Toner, J., and Sletten, R. (2013) The formation of Ca-Cl-rich groundwaters in the Dry Valleys of Antarctica: Field measurements and modeling of reactive transport. *Geochimica et Cosmochimica Acta,* **110**, 84-105.

Uchikawa, J., and Zeebe, R. (2012) The effect of carbonic anhydrase on the kinetics and equilibrium of the oxygen isotope exchange in the CO_2-H_2O system: Implications for $\delta^{18}O$ vital effects in biogenic carbonates. *Geochimica e Cosmochimica Acta,* **95**, 15-34.

Watkins, J., Nielsen, L., Ryerson, F., and DePaolo, D. (2013) The influence of kinetics on the oxygen isotope composition of calcium carbonate. *Earth and Planetary Science Letters,* **375**, 349-360.

Watkins, J., Hunt, J., Ryerson, F., and DePaolo, D. (2014) The influence of temperature, pH, and growth rate on the $\delta^{18}O$ composition of inorganically precipitated calcite. *Earth and Planetary Science Letters,* **404**, 332-343.

Wharton, R., Parker, B., Simmons, G., Seaburg, K., and Love, F. (1982) Biogenic calcite structures forming in Lake Fryxell, Antarctica. *Nature,* **295**, 403-405.

Wharton, R. (1994) Stromatolitic Mats in Antarctic Lakes. In *Phanerozoic Stromatolites II* (eds. J. Bertrand-Sarfati and C. Monty), 53-70.

Wostbrock, J., Brand, U., Coplen, T., Swart, P., Carlson, S., Brearley, A., and Sharp, Z. (2020) Calibration of carbonate-water triple oxygen isotope fractionation: Seeing through diagenesis in ancient carbonates. *Geochimica et Cosmochimica Acta,* **288**, 369-388.

Wostbrock, J., and Sharp, Z. (2021) Triple Oxygen Isotopes in Silica-Water and Carbonate-Water Systems. *Reviews in Mineralogy and Geochemistry,* **86**, 367-400.

Zeyen, N., Benzerara, K., Menguy, N., Brest, J., Templeton, A., Webb, S., Gérard, E., Moreira, D., López-Garciá, P., Tavera, R., and Morin, G. (2019) Fe-bearing phases in modern lacustrine microbialites from Mexico. *Geochimica et Cosmochimica Acta*, **253**, 201-230.